


RESEARCH ARTICLE

Extracellular vesicles derived from M2-like macrophages alleviate acute lung injury in a miR-709-mediated manner

Jie Yang¹ | Xiaofang Huang² | Qing Yu¹ | Shibo Wang³ | Xuehuan Wen¹ |
 Songjie Bai¹ | Lanxin Cao¹ | Kai Zhang¹ | Shufang Zhang⁴ | Xingang Wang⁵ |
 Zhanghui Chen⁶ | Zhijian Cai³  | Gensheng Zhang^{1,7} 

¹Department of Critical Care Medicine, Second Affiliated Hospital, Zhejiang University School of Medicine, Hangzhou, Zhejiang, China

²Department of Critical Care Medicine, Qilu Hospital of Shandong University, Jinan, Shandong, China

³Department of Orthopedics, Institute of Immunology, the Second Affiliated Hospital, Zhejiang University School of Medicine, Hangzhou, Zhejiang, China

⁴Department of Cardiology, Second Affiliated Hospital, Zhejiang University School of Medicine, Hangzhou, Zhejiang, China

⁵Department of Burns & Wound Care Centre, the Second Affiliated Hospital of Zhejiang University School of Medicine, the Key Laboratory of Trauma and Burns of Zhejiang University, Hangzhou, Zhejiang, China

⁶Zhanjiang Institute of Clinical Medicine, Zhanjiang Central Hospital, Guangdong Medical University, Zhanjiang, Guangdong, China

⁷Key Laboratory of Multiple Organ Failure (Zhejiang University), Ministry of Education, Hangzhou, Zhejiang, China

Correspondence

Xingang Wang, Department of Burns & Wound Care Centre, the Second Affiliated Hospital of Zhejiang University School of Medicine, the Key Laboratory of Trauma and Burns of Zhejiang University, Hangzhou, Zhejiang 310009, China.
 Email: wangxingang8157@zju.edu.cn

Zhanghui Chen, Zhanjiang Institute of Clinical Medicine, Zhanjiang Central Hospital, Guangdong Medical University, Zhanjiang 524045, China.
 Email: zjcell@126.com

Zhijian Cai, Department of Orthopedics, Institute of Immunology, the Second Affiliated Hospital, Zhejiang University School of Medicine, Hangzhou 310009, China.
 Email: caizj@zju.edu.cn

Gensheng Zhang, Department of Critical Care Medicine, Second Affiliated Hospital, Zhejiang University School of Medicine, Key Laboratory of Multiple Organ Failure (Zhejiang University), Ministry of Education, Hangzhou 310009, China.
 Email: genshengzhang@zju.edu.cn

Yang J and Huang XF contributed to the work equally.

Funding information

National Natural Science Foundation of China, Grant/Award Numbers: No.82270086, No.81971871, No.81971886, No.82170053; National

Abstract

Acute lung injury/acute respiratory distress syndrome (ALI/ARDS) is characterised by an uncontrolled inflammatory response, and current treatment strategies have limited efficacy. Although the protective effect of M2-like macrophages (M2 ϕ) and their extracellular vesicles (EVs) has been well-documented in other inflammatory diseases, the role of M2 ϕ -derived EVs (M2 ϕ -EVs) in the pathogenesis of ALI/ARDS remains poorly understood. The present study utilised a mouse model of lipopolysaccharide-induced ALI to first demonstrate a decrease in endogenous M2-like alveolar macrophage-derived EVs. And then, intratracheal instillation of exogenous M2 ϕ -EVs from the mouse alveolar macrophage cell line (MH-S) primarily led to a take up by alveolar macrophages, resulting in reduced lung inflammation and injury. Mechanistically, the M2 ϕ -EVs effectively suppressed the pyroptosis of alveolar macrophages and inhibited the release of excessive cytokines such as IL-6, TNF- α and IL-1 β both in vivo and in vitro, which were closely related to NF- κ B/NLRP3 signalling pathway inhibition. Of note, the protective effect of M2 ϕ -EVs was partly mediated by miR-709, as evidenced by the inhibition of miR-709 expression in M2 ϕ -EVs mitigated their protective effect against lipopolysaccharide-induced ALI in mice. In addition, we found that the expression of miR-709 in EVs derived from bronchoalveolar lavage fluid was correlated negatively with disease severity in ARDS patients, indicating its potential as a marker for ARDS severity. Altogether, our study revealed that M2 ϕ -EVs played a protective role in the pathogenesis of ALI/ARDS, partly mediated by miR-709, offering a potential strategy for assessing disease severity and treating ALI/ARDS.

This is an open access article under the terms of the [Creative Commons Attribution-NonCommercial License](https://creativecommons.org/licenses/by-nc/4.0/), which permits use, distribution and reproduction in any medium, provided the original work is properly cited and is not used for commercial purposes.

© 2024 The Authors. *Journal of Extracellular Vesicles* published by Wiley Periodicals LLC on behalf of International Society for Extracellular Vesicles.

Key Research and Development Program of China, Grant/Award Number: 2022YFC2403100; Natural Science Foundation of Shandong Province, Grant/Award Number: No.ZR202111020044; Key Research and Development Program of Zhejiang Province, Grant/Award Number: No.2024C03186

KEYWORDS

ALI/ARDS, alveolar macrophages, extracellular vesicles, M2 polarisation, miRNA, NLRP3 inflammasome

1 | INTRODUCTION

Acute lung injury/acute respiratory distress syndrome (ALI/ARDS) is a clinical syndrome caused by multiple causative factors, including sepsis, pneumonia, trauma, aspiration and acute pancreatitis, and characterised by deterioration of pulmonary inflammation and heightened microvascular permeability (Xia et al., 2022). Despite the mortality rate has been significantly reduced with lung-protective ventilation, there is currently no effective pharmacologic therapy (Rubinfeld et al., 2005). Thus, it is critical to develop new treatment strategies for ALI/ARDS.

The primary pathogenic mechanism of ALI/ARDS involves an inflammatory cascade triggered by an excessive inflammatory response (Aggarwal et al., 2014). In particular, inflammasomes play a crucial role, with nucleotides binding oligomeric domains like receptor protein 3 (NLRP3) inflammasome being the most important (Atianand et al., 2013). The NLRP3 inflammasome contains NLRP3, apoptosis-associated speck-like protein (ASC), and Pro-caspase-1, and its activation leads to caspase-1-dependent maturation and release of several proinflammatory cytokines, including IL-1 β and IL-18 (Atianand et al., 2013). Amounting research has found that NLRP3 inflammasome overactivation is closely related to various acute and chronic lung diseases, including respiratory infections, chronic obstructive pulmonary disease, asthma (De Nardo et al., 2014), as well as ALI/ARDS (Yang et al., 2019), consistent with our previous study (Yang et al., 2022). Hence, targeting the NLRP3 inflammasome may be effective in alleviating ALI/ARDS.

Macrophages serve as the essential innate immune cells participating in host defence against pathogens and tissue homeostasis. Although several types of macrophages are present in the lungs, alveolar macrophages are particularly abundant and play an essential role in immune responses (Kulikauskaitė & Wack, 2020). Generally, macrophages are heterogeneous immune cells and can be broadly categorised into M1-like macrophages (M1 ϕ) and M2-like macrophages (M2 ϕ) (Huang et al., 2018). M1 ϕ are primarily involved in proinflammatory processes, and are a major source of numerous cytokines including IL-6, TNF- α and IL-1 β , which contribute to tissue damage following infections (Wang et al., 2020). In contrast, M2 ϕ have been shown to play anti-inflammatory and tissue repair roles in mouse models of acute liver failure, acute kidney injury, colitis and ALI (Bai et al., 2021; Feng et al., 2023; Lin et al., 2014; Song et al., 2019; Tang et al., 2020), partly by inhibiting NLRP3 inflammasome activation (Bai et al., 2017; Bai et al., 2018; Bai et al., 2019). However, practical applications of macrophage-oriented cell therapy in vivo face several limitations. For example, the inherent high immunogenicity of macrophages restricts their source availability, and the propensity of macrophages to differentiate hinders the ability to maintain a steady phenotype upon their introduction into the body. Thus, more stable, convenient and safer alternatives are needed (Watanabe et al., 2021).

It has been reported that the effect of macrophages is partly mediated by the release of cytokines and extracellular vesicles (EVs) (Mao et al., 2020; Wang et al., 2020). Among them, EVs are a group of nanovesicles (30-1000 nm) secreted by living cells. EVs possess bioactive properties similar to donor cells due to the various biomolecules they carry from parental cells during biogenesis (Lou et al., 2021; Wang et al., 2020). Recent data suggest that M2 ϕ -derived EVs (M2 ϕ -EVs) exert the anti-inflammatory effect in various inflammatory diseases such as acute colitis, asthma and pneumonia (Hou et al., 2021; Zhang et al., 2020), but whether M2 ϕ -EVs can reduce lung injury in ALI/ARDS is yet to be explored.

Given the potent anti-inflammatory properties of M2 ϕ -EVs and the uncontrolled inflammation involved in ALI/ARDS pathogenesis, we hypothesised that M2 ϕ -EVs may attenuate lung inflammation and lung injury in ALI/ARDS. Herein, we aimed to investigate the potential protective role of M2 ϕ -EVs in ALI/ARDS along with the underlying mechanism.

2 | MATERIALS AND METHODS

2.1 | Human subjects and human sample collections

Human bronchoalveolar lavage fluid (BALF) sample collections and human cell experiments were approved by the Second Affiliated Hospital Ethics Committee (NO.20220124 and NO.20230022), which followed the recommendations of the Declaration of Helsinki for biomedical research involving human subjects. All subjects or their next of kin provided informed consent prior to enrolment. In total, sixteen patients with ARDS were enrolled according to the Berlin definition of ARDS (acute hypoxemia, partial pressure of arterial oxygen (PaO₂)/fraction of inspired oxygen (FiO₂) ratio <300 mmHg, and bilateral pulmonary infiltrates on chest radiography, and not explained by cardiac oedema) (Ranieri et al., 2012). Eight patients who previously had small pulmonary nodules requiring BALF as a routine physical examination were included as controls.

The BALF samples were collected from patients by flushing the lungs with 20 mL saline when clinically necessary and centrifuged at $800 \times g$ for 5 min at 4°C , and the cell pellets and supernatant were separated and stored at -80°C respectively for future analysis. Meanwhile, the baseline characteristics, demographic data, routine biochemical parameters and clinical variables were collected retrospectively. The basic information of patients is shown in Table S1.

2.2 | Mice

Male C57BL/6 mice (6–8 weeks old) were obtained from Shanghai SLAC Laboratory Animal Co., Ltd. (SCXK 2017-0005). Mice were maintained under specific pathogen-free conditions, and experimental protocols were reviewed and approved by the Ethics Committee for Animal Studies at Zhejiang University.

2.3 | Cell lines and cell culture

Murine MH-S cells (CRL-2019) were purchased from the American Type Culture Collection (Manassas, VA, USA), and acute monocytic leukaemia THP-1 cells (TCHu57) were purchased from the Type Culture Collection of the Chinese Academy of Sciences (Shanghai, China). Mouse primary peritoneal macrophages (MP-M ϕ) were isolated from mice as previously described (Xiu et al., 2021) and the isolation service of human primary CD14⁺ monocytes (HP-M ϕ) from peripheral blood mononuclear cells was provided by Milestone Biotechnology (Hangzhou, China). MH-S and THP-1 cells, as well as MP-M ϕ and HP-M ϕ , were cultured in RPMI-1640 (Basalmedia) supplemented with 10% FBS (Thermo Fisher Scientific) and 1% penicillin/streptomycin, respectively. Among them, additional phorbol myristate acetate (PMA, 50 ng/mL, Sigma-Aldrich), and recombinant human macrophage colony stimulating factor (hM-CSF, 20 ng/mL, MCE) were added to the culture medium of THP-1 cells and HP-M ϕ , respectively. All cells were cultured at 37°C with 5% CO_2 . MH-S cells and MP-M ϕ were induced to M2 ϕ and MP-M2 ϕ by incubating with recombinant mouse IL-4 protein (mIL-4, 20 ng/mL, Miltenyi) for 24 h. THP-1 cells and HP-M ϕ were induced to T-M2 ϕ and HP-M2 ϕ by incubating with recombinant human IL-4 protein (hIL-4, 20 ng/mL, Miltenyi) for 24 h. M2 ϕ /T-M2 ϕ /MP-M2 ϕ /HP-M2 ϕ were washed with PBS and cultured in EV-depleted medium for another 24 h for collection of the conditioned medium.

2.4 | In vivo lipopolysaccharide-induced acute lung injury model

Pathogen-free, 8-week-old male C57BL/6 mice were used to establish a lipopolysaccharide (LPS)-induced ALI model. In brief, mice were anaesthetised by isoflurane inhalation, the skin and muscles were incised sequentially to expose the trachea, and 25 μL of 1 mg/kg LPS (O55:B5, Sigma, USA) was slowly injected into the lungs from the distal end of the trachea using a microinjector.

To detect the dynamic changes in BALF-derived EVs (BALF-EVs), mice were sacrificed at 6 or 24 h after LPS administration. For EV treatments, 30 min after LPS infection, 100 μg M2 ϕ -EVs, negative control (NC) inhibitor-M2 ϕ -EVs, miR-709 inhibitor-M2 ϕ -EVs or M0 ϕ -EVs in 50 μL PBS was administered through the tracheal and 24 h after LPS administration, mice were euthanised by intraperitoneal injection of pentobarbital, and lung tissues and BALF were taken for analysis.

In the groups mentioned above for different detection, mice that did not receive LPS stimulation or EV treatments were given an equivalent volume of PBS through airway infusion as control at the corresponding time.

2.5 | Histopathology

The lungs were dissected from individual mice, immediately fixed with 4% paraformaldehyde, and then subjected to haematoxylin and eosin (H&E) staining. At least three images of randomly selected microscopic fields were captured from each slide from each mouse. The severity of ALI was assessed by inflammatory cell infiltration and alveolar wall thickening.

2.6 | Separation of EVs

The conditioned medium, human BALF samples or mouse BALF samples were collected and centrifuged at $300 \times g$ for 10 min, $2000 \times g$ for 20 min and $10,000 \times g$ for 30 min at 4°C . Then, the centrifuged samples were filtered through a 0.22 μm pore polyethersulfone (PES) membrane filter system (Corning, New York, NY), and EVs were then isolated by two methods: ultracentrifugation (UC) and size exclusion chromatography (SEC).

For the UC method, the samples were spun at $120,000 \times g$ for 90 min at 4°C on an Optima XPN-100 ultracentrifuge with a SW32Ti rotor (Beckman Coulter, Brea, CA, USA). The isolated EVs were washed with PBS and subjected to secondary centrifugation ($120,000 \times g$ for 90 min at 4°C). The pure EV pellets were resuspended in PBS and stored at -80°C for further use.

For the SEC method, the samples were concentrated by a 100 kDa molecular weight cutoff centrifugal filter (Merck Millipore, Billerica, MA, USA) to reach a volume less than 500 μL and then subjected to qEV columns according to the manufacturer's protocol (Izon Science, Christchurch, New Zealand). The fraction 7–9 were collected jointly as 'EV fractions' and further concentrated using 10 kDa filters before use.

It should be noted that EVs such as M0 φ -EVs^{SEC} and M2 φ -EVs^{SEC} were specifically labelled to indicate that they were extracted by SEC method, but the remaining EVs were usually obtained by UC method. In addition, the protein contents of EVs were quantified using a BCA protein assay kit in the absence of detergent (Thermo Fisher Scientific).

2.7 | Western blotting

Total protein was extracted using RIPA buffer (Beyotime, Shanghai, China) or cell lysis buffer (CST, USA) containing 1 mM phenylmethylsulfonyl fluoride (PMSF) and protease inhibitor cocktail. Protein concentrations were determined by the BCA protein assay kit. A total of 10 μg of the indicated EVs, cell lysates or tissue lysates were resuspended in $5 \times$ SDS loading buffer, subsequently incubated at 100°C for 10 min. Then, the supernatant was separated by 10% SDS-polyacrylamide gel (Thermo Fisher Scientific) electrophoresis and transferred to PVDF membranes (Millipore), which were blocked with 5% non-fat powdered milk in PBS with Tween 20 buffer (PBST) for 1 h, incubated with the relevant primary antibodies at 4°C overnight, and then incubated with secondary antibodies at RT for 1 h. An ECL kit (MultiSciences, Hangzhou, Zhejiang, China) was used to detect the bands. The antibodies used and the corresponding dilutions are listed in Table S2.

2.8 | Transmission electron microscopy

5 μg of the indicated EVs were diluted in PBS and placed on 200-mesh carbon-coated copper grids at RT for 1 min. The excess suspension was removed using filter paper. Then, the EVs were negatively stained with uranyl acetate at RT for 1 min, washed twice with PBS, dried and examined under a Talos L120C G2 electron microscope (Thermo Scientific, USA) operating at 120 kV.

2.9 | Nanoparticle tracking analysis

The number and size distribution of the indicated EVs were analysed using the NanoSight NS500 (Malvern, Malvern, Worcestershire, UK).

2.10 | Immunofluorescence and confocal microscopy

The cells were washed and fixed in prechilled methanol for 10 min and then permeabilised with 0.1% Triton X-100 for another 10 min. After blocking with 5% BSA, the cells were incubated overnight at 4°C with different primary antibodies, followed by the corresponding secondary antibodies. Nuclei were stained with DAPI (Invitrogen, Carlsbad, CA). Images of the cells were captured with an Olympus confocal fluorescence microscope (Olympus, Tokyo, Japan). The antibodies used and the corresponding dilutions are listed in Table S2.

2.11 | The binding of EVs and LPS in vitro

10 μg M0 φ -EVs or M2 φ -EVs were mixed with FITC-LPS (Sigma, USA) according to these different ratios of 10:0.5–10:64 for 1 h at 37°C in PBS, with a final volume of 100 μL (Kumari et al., 2023). For detection of the binding ability of EVs and LPS by flow cytometry, all the unbound LPS in each mixture was removed by UC at $120,000 \times g$ for 30 min at 4°C , and the pellets were resuspended in PBS for further analysis; for detection of the effect of EV-bound LPS, the above mixtures of EVs and LPS, LPS or LPS transfection were directly added to MH-S cells for 24 h. After incubation, the treated cells and supernatant were collected for further analysis.

2.12 | EV labelling

EVs were labelled using VivoTrack 680 (Fluorescence, Beijing, China), PKH26 (Sigma-Aldrich) or carboxyfluorescein succinimidyl ester (CFSE, Thermo Fisher Scientific) according to the manufacturer's instructions. For VivoTrack 680 labelling, 100 μg EVs in 200 μL PBS were mixed with 42 μM VivoTrack 680 at RT for 30 min. For PKH26 labelling, 100 μg EVs were resuspended in 250 μL diluent C, 1 μL PKH26 ethanolic dye solution was added into another 250 μL diluent C. Then, the EV suspension was mixed with the dye solution for 15 min at RT. For CFSE labelling, 100 μg EVs in 200 μL PBS were incubated with 7.5 μM CFSE at 37°C for 4 min. The staining was stopped by adding an equal volume of EV-depleted FBS and incubating for another 1 min. Finally, all the unbound dye was removed by UC at 120,000 $\times g$ for 30 min at 4°C, and the pellets were resuspended in different volumes of PBS according to the specific circumstances.

2.13 | In vivo biodistribution of EVs in mice

C57BL/6 mice were pretreated with 1 mg/kg LPS or PBS intratracheally for 30 min, then VivoTrack 680-labelled M2 ϕ -EVs (100 μg in 50 μL PBS per mouse) were intratracheally injected into the above C57BL/6 mice. Twenty-four hours later, the mice were sacrificed by an overdose of pentobarbital sodium anaesthesia, and the organs including the brain, heart, lungs, liver, kidneys, spleen and gastro-intestinal tract were collected and observed using an in vivo imaging system (IVIS, Perkin Elmer, Waltham, MA, USA). The fluorescence intensity was quantified by Analyze 12.0 software (Perkin Elmer). To further detect the distribution of EVs in different cell types in lung tissues or BALF, C57BL/6 mice were pretreated with 1 mg/kg LPS or PBS intratracheally for 30 min, then CFSE-labelled M2 ϕ -EVs (100 μg in 50 μL PBS per mouse) were intratracheally injected into the above C57BL/6 mice. Twenty-four hours later, the mice were sacrificed by an overdose of pentobarbital sodium anaesthesia. Among them, half of the mice were used for lung tissue flow cytometry, and the lung tissues were dissected from mice, washed extensively in PBS, minced and incubated with 1 mg/mL collagenase type IV (Worthington Biochemical Corp., USA), and 0.1 mg/mL DNase I (Sigma, USA) in RPMI-1640 medium for 60 min at 37°C with shaking (150 r. p.m.). The cell suspension was filtered through a 70- μm cell strainer, and red blood cells were lysed using red blood cell lysis buffer (Sigma, USA). Besides, the rest half of the mice were taken for BALF flow cytometry, 400 μL of PBS was instilled into the trachea, and BALF was collected by repeated irrigation, and this step was repeated three times. The collected single-cell suspension from lung tissues and BALF were taken for flow cytometry.

2.14 | Cellular uptake assay of EVs

MH-S cells were incubated with PKH26-labelled M2 ϕ -EVs (10 $\mu\text{g}/\text{mL}$) for 0, 0.5, 1 and 2 h at 37°C with 5% CO₂. After incubation, the cells were washed twice with PBS and analysed by flow cytometry.

2.15 | In vitro inflammasome model and EV treatments

MH-S cells, PMA-induced THP-1 cells, MP-M ϕ and hM-CSF-included HP-M ϕ were treated with 0.5 $\mu\text{g}/\text{mL}$ LPS for 24 h and ATP (0.5 mM, MCE) for 30 min at 37°C with 5% CO₂ to activate NLRP3 inflammasome. M2 ϕ -EVs, M2 ϕ -EVs^{SEC}, T-M2 ϕ -EVs, MP-M2 ϕ -EVs and HP-M2 ϕ -EVs were added 30 min after LPS treatment for functional evaluation of EVs. After incubation, the treated cells and supernatant were collected for further analysis.

2.16 | Flow cytometric analysis

As previously described, EVs were captured by 4 μm -diameter aldehyde/sulphate latex beads (Thermo Fisher Scientific) (Jiang et al., 2016). Briefly, 20 μg of EVs were incubated with 5 μL of beads for 30 min at RT in PBS, with a final volume of 100 μL . Then, 100 μL of EV-depleted FBS was added to incubate another 30 min. Cells or EV-coated beads were washed in PBS with 1% BSA and collected by centrifugation at 800 $\times g$ or 3800 $\times g$ for 5 min at 4°C, respectively. Then, the cells or beads were incubated with the corresponding fluorescence-labelled antibodies in 100 μL of PBS for 30 min at RT. After three washes in PBS, cells or beads were analysed by flow cytometry (CytoFlex flow cytometer, Beckman Coulter, Brea, CA, USA), and the data were analysed using FlowJo software (TreeStar, Ashland, OR, USA). The cells or beads were initially gated based on FSC-A and SSC-A to exclude debris and dead cells and then gated based on SSC-A and SSC-H to exclude doublets and aggregates. The fluorescent-positive cells or beads were gated in the appropriate fluorescent channels. The antibodies used are listed in Table S2.

2.17 | ELISA analysis of cytokine levels

The interleukin-6 (IL-6), tumour necrosis factor- α (TNF- α) and interleukin-1 β (IL-1 β) in cell supernatant or BALF samples were measured by ELISA (Thermo Fisher Scientific) according to the manufacturer's instructions.

2.18 | RNA extraction and real-time PCR analysis

Total RNA was isolated from EVs or cells with TRIzol (Thermo Fisher Scientific). Reverse transcription was performed with a Reverse Transcription Kit (Toyobo, Osaka, Japan). For reverse transcription of mature miRNAs, specific primers of mmu-miR-5107-5p, mmu-miR-511-3p, mmu-miR-709, mmu-miR-378d, mmu-miR-125b-2-3p, mmu-miR-682-3p, mmu-miR-350-5p and U6 (GenePharma, Shanghai, China) were used; for reverse transcription of mRNAs, primers in Reverse Transcription Kit (Toyobo) were used. PCR analysis was performed with Power SYBR Green (TaKaRa, Dalian, Liaoning, China) by using the following reaction conditions: 95°C for 30' followed by 39 cycles of 95°C for 5' and 60°C for 30'. For detection of miRNA expression, U6 snRNA served as an internal control. For mRNA detection, Gapdh served as an internal control. The relative fold changes in the expression levels of miRNAs or mRNAs were calculated using the following equation: relative quantification = $2^{-\Delta\Delta CT}$. The primers used are listed in Table S3.

2.19 | Transfection of siRNA

The MH-S cells were incubated with 20 ng/mL mIL-4 protein for 24 h and then transfected with 100 nM NC siRNA or Dicer siRNA for 24 h using Mirus Transfection reagent (Polyplus, Beijing, China) according to the manufacturer's instructions. Then, the conditioned medium was collected for EV extraction, and Dicer's cell silence was measured by qPCR and western blotting. The siRNAs were synthesised by GenePharma, and the sequences are listed in Table S3.

2.20 | Transfection of miRNA

For collection of EVs, the MH-S cells were incubated with 20 ng/mL mIL-4 protein for 24 h and then transfected with 100 nM NC inhibitors or miR-709 inhibitors for 24 h using Mirus Transfection reagent according to the manufacturer's instructions. Then, the conditioned medium was collected for EV extraction, and the silence of miR-709 in cells and EVs was measured by qPCR. To detect the effect of miR-709 mimics, MH-S cells or PMA-induced THP-1 cells were pretreated with 0.5 μ g/mL LPS for 30 min and then transfected with 100 nM NC mimics or miR-709 mimics using Mirus Transfection reagent according to the manufacturer's instructions for 23 h and then subjected to 0.5 mM ATP for another 30 min. The supernatant and cell pellets were collected for further analysis. The miRNAs were synthesised by GenePharma, and the sequences are listed in Table S3.

2.21 | Sequencing of miRNAs in EVs and data analysis

Total RNA was extracted from M0 ϕ -EVs and M2 ϕ -EVs and the final ligation PCR products were sequenced using an Illumina HiSeq™ 2000 machine (LC-Bio Technology Co., Ltd., Hangzhou, China). The expressed miRNAs with criteria of $|\text{Log}_2(\text{fold change})| > 1$ and p -value < 0.05 were considered significantly different.

2.22 | Statistical analyses

All data are expressed as the mean \pm SD. Statistical analyses were performed with GraphPad Prism 8.0 software. Unpaired Student's t -test was used to analyse the differences between two groups, and differences among three or more groups were analysed by one-way analysis of variance (ANOVA) or two-way ANOVA followed by a post hoc Tukey test. Overall survival and post-progression survival were assessed by Kaplan-Meier analysis. A value of $p < 0.05$ was considered statistically significant.

3 | RESULTS

3.1 | The M2/M1 phenotype of alveolar macrophage-derived EVs was suppressed during LPS-induced ALI

To investigate the dynamic changes in alveolar macrophage-derived EVs (AM-EVs) during the period of ALI/ARDS, a mouse model of ALI was established by intratracheal instillation of LPS and lung injury indicators were observed at 6 and 24 h after LPS administration. H&E staining of lung tissues showed increased bleeding, inflammatory cell infiltration and alveolar wall thickening in mice with prolonged LPS exposure (Figure S1A). Meanwhile, the protein accumulation (Figure S1B) and the release of IL-1 β cytokine (Figure S1C) in the BALF of mice reached a peak at 24 h, whilst IL-6 and TNF- α levels elevated at 6 h, followed by a decline at 24 h (Figure S1C). In addition, flow cytometry showed that the recruitment of neutrophils in BALF increased significantly (Figure S1D). The above results suggested that the lung tissue injury of mice progressively worsened as the exposure to LPS was prolonged, indicating the successful establishment of the ALI model.

Given the pivotal role of alveolar macrophages in ALI, we initially assessed alterations in alveolar macrophage abundance by flow cytometry and observed a significant reduction in the number of alveolar macrophages (Figure 1a). Subsequently, we proceeded to examine the polarisation markers CD86 (M1-related marker) and CD206 (M2-related marker) on alveolar macrophages, and found a time-dependent decrease in the ratio of M2/M1-like alveolar macrophages (Figure 1b), suggesting that the polarisation of alveolar macrophages in BALF was changed during ALI. Then BALF-EVs that obtained from mice were examined using transmission electron microscopy (TEM) and these captured EVs in all groups had a typical cup shape (Figure 1c). The size and count of BALF-EVs were determined using nanoparticle tracking analysis (NTA). Although there were no significant size differences among the three groups (Figure 1d), the quantity of BALF-EVs gradually decreased with extended LPS administration (Figure 1e). We then focused on the changes of AM-EVs present in BALF. Flow cytometry was used to demonstrate a reduction in the percentage of AM-EVs in BALF at 6 and 24 h following LPS instillation compared to baseline, whilst no difference was observed between these two time points (Figure 1f). Further polarisation analysis of AM-EVs revealed a gradual increase in the proportion of M1-like AM-EVs, whilst the percentage of M2-like AM-EVs gradually decreased over time following LPS instillation. Thus, the ratio of M2/M1-like AM-EVs decreased sharply (Figure 1g), similar to the changes observed in alveolar macrophages. These results indicated that as lung tissue damage worsened in LPS-induced ALI mice, there was a decline in the number of AM-EVs, with a predominant shift towards an M1 phenotype.

3.2 | Purification, isolation and characterisation of M2 ϕ -EVs

It is well-documented that exogenous M2 ϕ supplementation can improve ALI (Liu et al., 2019), so we wondered whether supplementing exogenous M2 ϕ -EVs to rescue the decline in endogenous M2-like AM-EVs ratio during ALI would have the same protective effect. Due to the poor extraction efficiency and low EV production of primary alveolar macrophages in mice, we mainly opted to use the mouse alveolar macrophage cell line (MH-S) for the subsequent experiments. We treated initial MH-S cells (M0 ϕ) with IL-4 for M2 polarisation (Huang et al., 2022) and found that the M2 ϕ -specific biomarkers CD206 and Arg-1 were significantly expressed (Figure S2A–C). The EVs were further extracted from the culture medium of M0 ϕ and M2 ϕ for identification. According to TEM and NTA, both M0 ϕ -EVs and M2 ϕ -EVs exhibited distinct biconcave morphological features of EVs (Figure S2D), with an average particle size of approximately 165.7 and 157.2 nm, respectively (Figure S2E). Both M0 ϕ -EVs and M2 ϕ -EVs showed positive expressions of Alix, TSG101, Syntenin and CD9 (Figure S2F). Moreover, Calnexin and PDI were only detected in cell lysates, which originated from the endoplasmic reticulum and were considered as negative markers for EVs (Figure S2F). Based on the above results, there seemed to be no significant differences between these two types of EVs, as they both exhibited typical characteristics. However, further investigation revealed that specific biomarkers CD206 and Arg-1 were overexpressed in M2 ϕ -EVs rather than M0 ϕ -EVs (Figure S2F), similar to their parental cells. Overall, these results implied the successful preparation of exogenous M2 ϕ -EVs.

3.3 | M2 ϕ -EVs alleviated LPS-induced ALI in mice

Prior to exploring the role of M2 ϕ -EVs in ALI, we first identified the *in vivo* distribution of these vesicles. Previous studies have indicated that the intravenously injected EVs tend to accumulate in the liver and are mostly taken up by phagocytes including macrophages *in vivo* (Zhang et al., 2020). However, in our study, M2 ϕ -EVs were delivered by intratracheal instillation. As shown by fluorescence imaging, the intratracheally injected M2 ϕ -EVs were primarily localised within lung tissues, with minimal presence in other organs regardless of LPS stimulation (Figure 2a). Flow cytometry analysis of lung tissues (Figure 2b) and BALF (Figure 2c) demonstrated that the pulmonary neutrophils exhibited a slight increase in uptake of M2 ϕ -EVs following LPS

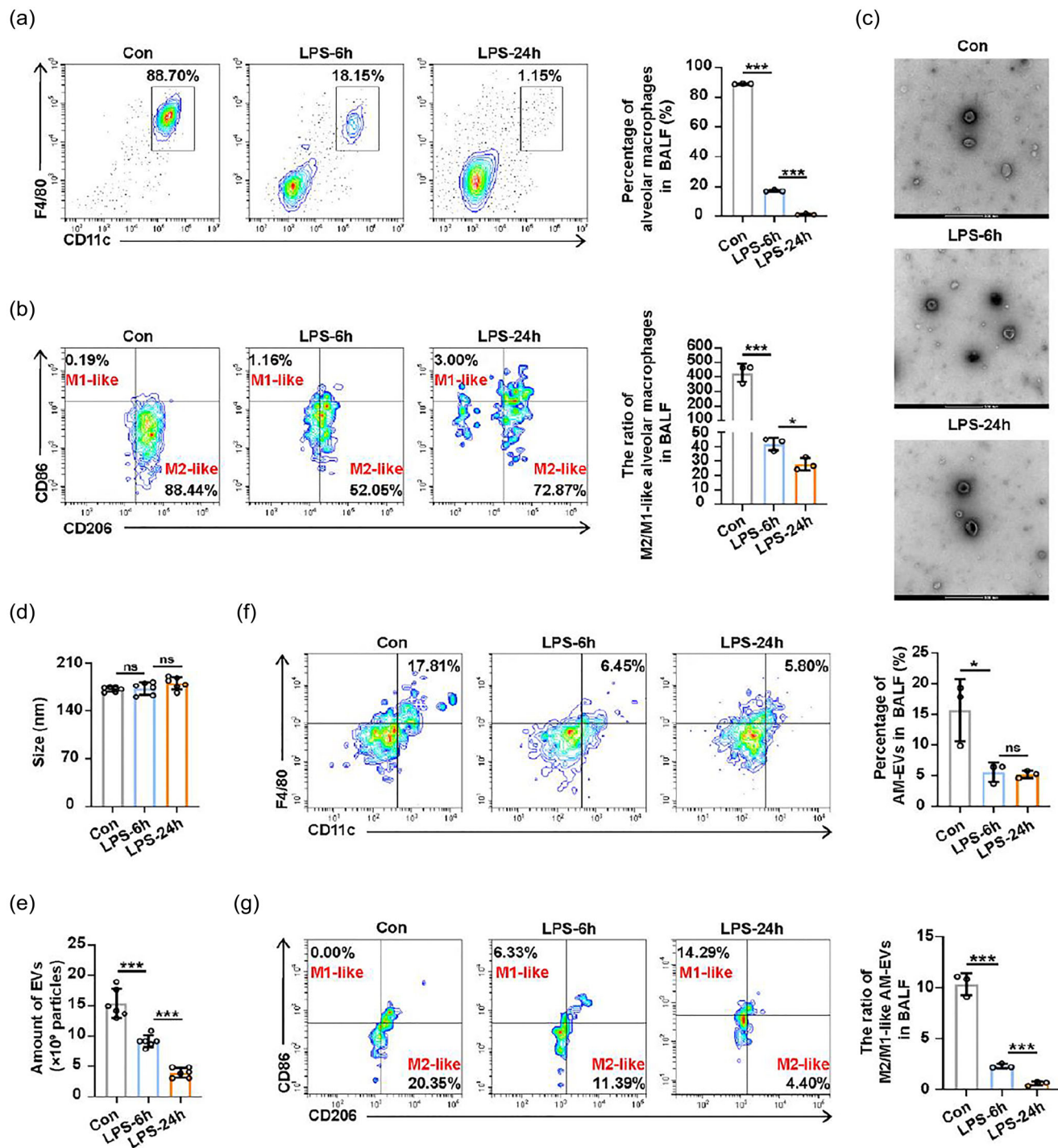


FIGURE 1 The dynamic changes in M2/M1-like alveolar macrophages and their derived EVs in mice model of LPS-induced ALI. Mice were treated intratracheally with 1 mg/kg LPS for 6 and 24 h. The BALF from the indicated time points were obtained for further analysis. (a and b) Flow cytometry analysis for total percentage of alveolar macrophages (a) and the ratio of M2/M1-like alveolar macrophages (b) in BALF. (c) TEM images of BALF-EVs. (d and e) The diameter (d) and the number (e) of BALF-EVs isolated from mice were measured using NTA. (f and g) Flow cytometry analysis for the percentage of AM-EVs (f) and the ratio of M2/M1-like AM-EVs (g) in BALF. Representative results from three independent experiments are shown ($n = 3$ except for $n = 6$ in d, e). Scale bar, 200 nm. ns, not significant, * $p < 0.05$, *** $p < 0.001$ (one-way ANOVA test; mean \pm SD).

administration. In contrast, the internalisation of M2 ϕ -EVs by alveolar macrophages and pulmonary epithelial cells showed variable decrease. Nevertheless, M2 ϕ -EVs were mainly engulfed by alveolar macrophages rather than pulmonary neutrophils or pulmonary epithelial cells in both M2 ϕ -EVs group and LPS + M2 ϕ -EVs group (Figure 2b,c), indicating that alveolar macrophages might serve as the main target cells for the in vivo effect of M2 ϕ -EVs.

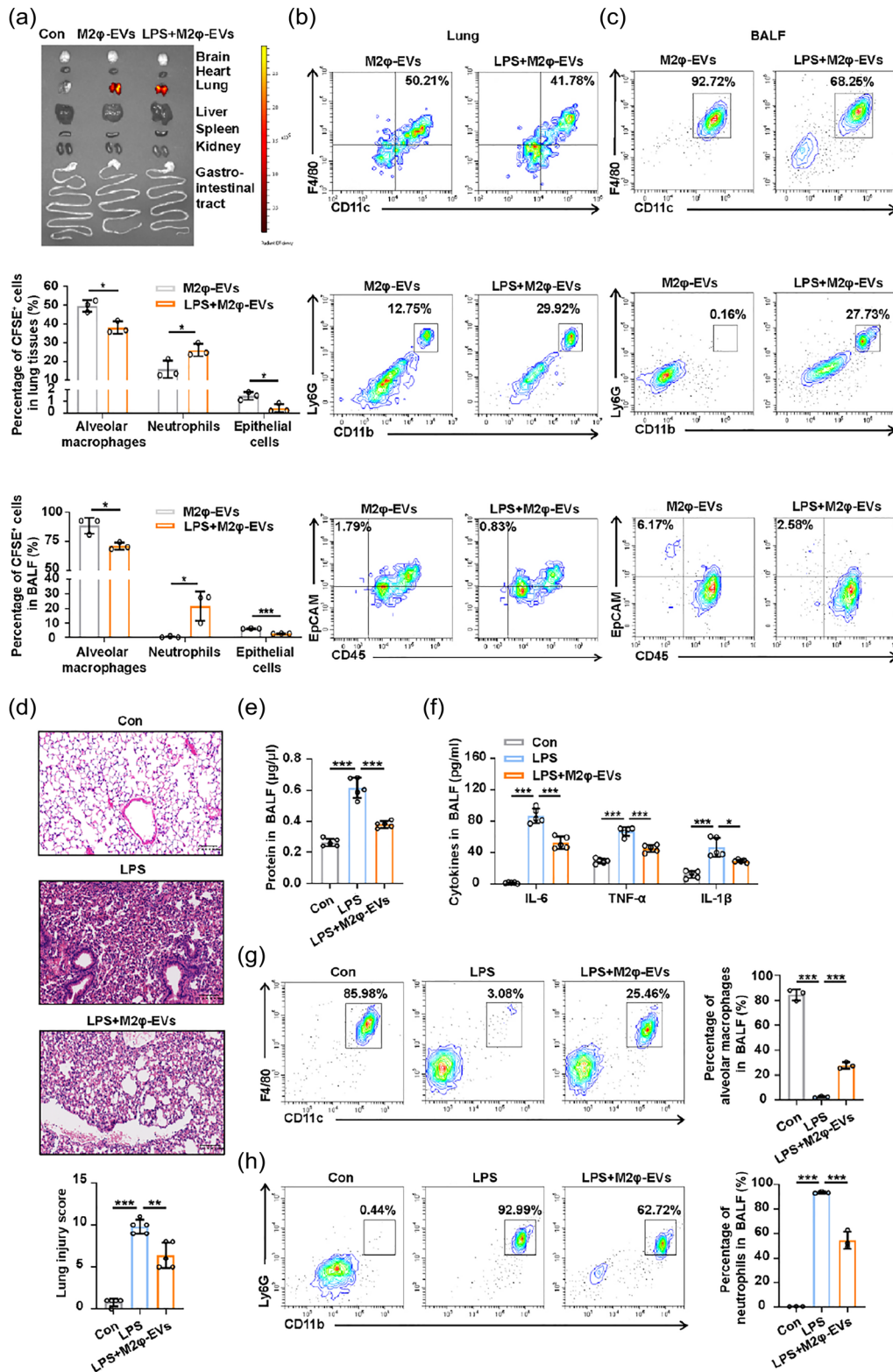


FIGURE 2 Exogenous M2φ-EV administration alleviated lung inflammation and injury in LPS-induced ALI mice. C57BL/6 mice were pretreated with 1 mg/kg LPS or PBS intratracheally for 30 min. (a) LPS-pretreated or PBS-pretreated mice were given 100 μg VivoTrack 680-labelled M2φ-EVs intratracheally, and the distribution of M2φ-EVs in the indicated organs was detected using an in vivo imaging system at 24 h after LPS/PBS administration. (b and c) LPS-pretreated or PBS-pretreated mice were given 100 μg CFSE-labelled M2φ-EVs intratracheally and sacrificed at 24 h after LPS/PBS administration. Flow cytometry analysis of alveolar macrophages, neutrophils and epithelial cells in lung tissues (b) and BALF (c) was performed to track the CFSE-labelled M2φ-EVs. (d–h) LPS-pretreated mice were injected intratracheally with 100 μg M2φ-EVs, and further experiments were performed at 24 h after LPS administration. (d) Representative H&E staining of lung tissues and pathological damage score. (e) The total protein concentration in BALF was detected by the BCA protein assay. (f) The concentrations of IL-6, TNF-α and IL-1β in BALF were measured by ELISA. (g and h) Flow cytometry analysis of alveolar macrophages (g) and neutrophils (h) in BALF. Representative results from three independent experiments are shown ($n = 3$ except for $n = 5$ in d, e, f). Scale bar, 100 μm. * $p < 0.05$, ** $p < 0.01$, *** $p < 0.001$ (one-way ANOVA test except for unpaired Student t -test in b, c; mean \pm SD).

We next established an *in vivo* mouse model of ALI and found that the intratracheal instillation of M2 ϕ -EVs alleviated LPS-induced lung damage evidenced by reduced inflammatory cell infiltration and alveolar wall thinning (Figure 2d), as well as a decrease in total protein concentration (Figure 2e) and levels of proinflammatory cytokines, including IL-6, TNF- α , IL-1 β (Figure 2f) in BALF. Moreover, the application of M2 ϕ -EVs increased the percentage of alveolar macrophages in BALF (Figure 2g), whilst the amount of proinflammatory neutrophils was decreased (Figure 2h). Thus, these data collectively revealed the dominant distribution of M2 ϕ -EVs in the lungs, especially in alveolar macrophages when administrated via airway infusion, and exogenous M2 ϕ -EVs elicited the anti-inflammatory effect and played a tissue-protective role during LPS-induced ALI.

3.4 | M2 ϕ -EVs inhibited the activation of the NLRP3 inflammasome

Since we have previously demonstrated that M2 ϕ -EV application can reverse LPS-induced alveolar macrophage depletion (Figure 2g) in the pathogenesis of ALI, we hypothesised that the high uptake of M2 ϕ -EVs by alveolar macrophages (Figure 2b,c) might inhibit their death. As pyroptosis of macrophages was critical during the development of ALI, as we previously described (Yang et al., 2022), we investigated whether the protective effect of M2 ϕ -EVs was related to the inhibition on NLRP3 inflammasome signalling pathway in alveolar macrophages. Initially, we co-incubated MH-S cells with PKH26-labelled M2 ϕ -EVs and noticed that M2 ϕ -EVs could be internalised by MH-S cells gradually, peaking at approximately 2 h, with more than 90% PKH26⁺ cells were observed (Figure 3a). Next, an *in vitro* inflammasome activation model was established in MH-S cells by administration of LPS + ATP, with or without the presence of M2 ϕ -EVs. The results showed that M2 ϕ -EV administration reduced the percentage of AnnexinV⁺/PI⁺ cells (Figure 3b). The above results, however, could not completely account for the occurrence of pyroptosis. Therefore, we further examined the expression levels of Pro-caspase-1 and Cle-caspase-1 in MH-S cells since the cleavage of Pro-caspase-1 is a critical step for activating NLRP3 inflammasome (Song et al., 2016). It was found that compared to the LPS + ATP group, M2 ϕ -EV treatment significantly downregulated the protein levels of Cle-caspase-1 (Figure 3c). In addition, M2 ϕ -EVs reduced the number of ASC specks stimulated by LPS + ATP (Figure 3d), a typical sign of NLRP3 inflammasome activation (Zhao et al., 2019).

However, it is worth noting that although M2 ϕ -EVs had been shown to effectively inhibit the activation of NLRP3 inflammasome in the aforementioned experiments, the latest research reported that EVs had an intrinsic capacity to bind bacterial LPS, leading to non-canonical activation of NLRP3 inflammasome by conferring cytosolic access for LPS (Kumari et al., 2023). Thus, in order to gain a relatively comprehensive understanding of the effect of M2 ϕ -EVs, we first tested the binding ability of EVs and LPS. Based on the ratios of EVs to LPS used in our study (10:0.5 *in vitro* and 10:2 *in vivo*), we preset a series of gradients. The results showed that the binding ability of either M0 ϕ -EVs or M2 ϕ -EVs with LPS was very weak for that even at a high ratio of 10:64, the percentage of FITC-LPS positive in M0 ϕ -EVs and M2 ϕ -EVs was only 3.94% and 3.5%, respectively (Figure S3A). Subsequently, to further explore whether EV-bound LPS could promote non-canonical activation of NLRP3 inflammasome in our study, we first co-cultured EVs and LPS for 1 h *in vitro* at different ratios of 10:0.5–10:64 to promote the binding of EVs and LPS, and then the above mixtures of EVs and LPS were each added to MH-S cells so that these EVs and LPS can continue to bind to each other in cell supernatant, thereby allowing more EVs to carry more LPS into the cytoplasm to activate the non-canonical NLRP3 inflammasome. However, our results showed that none of the mixtures of EVs and LPS mentioned above were effective to cleave Gasdermin D (GSDMD) (Figure S3B), nor could they cause the release of IL-1 β (Figure S3C), indicating that EV-bound LPS was not sufficient to trigger intracellular non-canonical activation of NLRP3 inflammasome at these incubation ratios in the current study. Thus, there was no need to consider the binding of EVs and LPS or the extra effect caused by EV-bound LPS in our study.

It is reported that the cellular expression of NLRP3 inflammasome components is vital for its assembly and activation (Song et al., 2020). We then examined the effect of M2 ϕ -EVs on expressions of NLRP3, ASC, and Pro-caspase-1 in MH-S cells. The results showed that M2 ϕ -EVs only reduced the LPS + ATP induced upregulation of NLRP3 protein levels, whilst ASC and Pro-caspase-1 proteins were expressed in a compositional manner, with their protein levels unaffected by LPS+ ATP or M2 ϕ -EVs (Figure 3e). Further qPCR analysis revealed that M2 ϕ -EVs attenuated the LPS + ATP induced increase in mRNA levels of NLRP3 (Figure 3f). Moreover, in line with the results *in vivo*, LPS + ATP stimulation induced remarkable expressions of proinflammatory cytokines including IL-6, TNF- α and IL-1 β , whereas they were reduced by M2 ϕ -EV treatment (Figure 3g,h). We further validated these findings *in vivo*, and the results showed that M2 ϕ -EV treatment effectively reduced the LPS-induced increases in the levels of Cle-caspase-1 protein (Figure 3i), as well as NLRP3 protein and mRNA expressions (Figure 3j,k) in lung tissues of ALI mice. These observations suggested that M2 ϕ -EVs inhibited the activation of the NLRP3 inflammasome and simultaneously decreased the secretion of proinflammatory cytokines including IL-6 and TNF- α both *in vivo* and *in vitro*.

To independently validate the protective effect of M2 ϕ -EVs, we employed another EV isolation method that rely on a different principle. First, we isolated M0 ϕ -EVs^{SEC} and M2 ϕ -EVs^{SEC} from the conditioned culture medium by SEC via qEV columns respectively (Figure S4A–C). Then, the extracted M2 ϕ -EVs^{SEC} were incubated with the MH-S cells induced by LPS + ATP to identify their anti-inflammatory effect. And we found that the treatment of M2 ϕ -EVs^{SEC} also reduced the release of IL-6, TNF- α and IL-1 β (Figure S4D,E), and down-regulated the elevated expression levels of NLRP3 protein and mRNA in MH-S cells induced

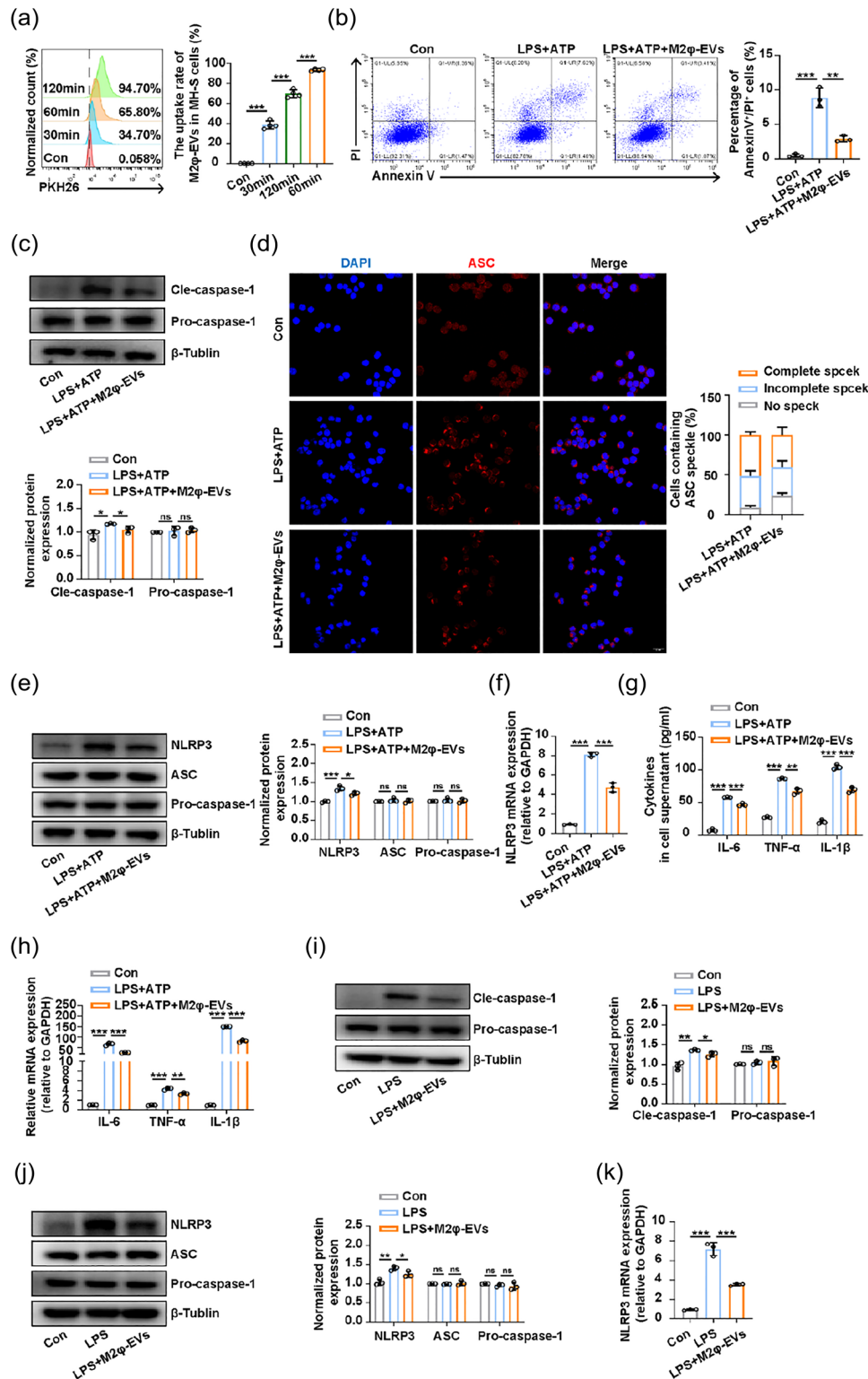


FIGURE 3 M2φ-EV treatment suppressed the activation of the NLRP3 inflammasome. (a) The uptake rate of PKH26-labelled M2φ-EVs by MH-S cells at different time points was measured by flow cytometry. (b–h) After LPS (0.5 μg/mL) stimulation for 30 min, MH-S cells were treated with M2φ-EVs (10 μg/mL) for 23 h and then subjected to ATP (0.5 mM) for another 30 min. (b) Flow cytometry analysis of the pyroptosis of MH-S cells (Annexin⁺/PI⁺). (c) Western blotting analysis of Pro-caspase-1, Cle-caspase-1 levels in MH-S cells. The histogram showed the relative ratio of the expression levels of the target protein to that of an internal reference. (d) The ASC speck formation was visualised by immunofluorescence analysis in MH-S cells. The histogram represented the quantification of the number of ASC specks. (e) Western blotting analysis of NLRP3, ASC and Pro-caspase-1 levels in MH-S cells. The histogram showed the relative ratio of the expression levels of the target protein to that of an internal reference. (f) The mRNA expression of NLRP3 in MH-S cells was analysed by qPCR. (g) The concentrations of IL-6, TNF-α and IL-1β in cell supernatant were measured by ELISA. (h) The mRNA expressions of IL-6, TNF-α and IL-1β in MH-S cells were analysed by qPCR. (i–k) C57BL/6 mice were pretreated with LPS at a dosage of 1 mg/kg intratracheally for 30 min and then injected intratracheally with 100 μg M2φ-EVs, and mice were sacrificed at 24 h after LPS administration for further experimental analysis. (i) Western blotting analysis

(Continues)

FIGURE 3 (Continued)

of Pro-caspase-1, Cle-caspase-1 levels in lung tissues. The histogram showed the relative ratio of the expression levels of the target protein to that of an internal reference. (j) Western blotting analysis of NLRP3, ASC and Pro-caspase-1 levels in lung tissues. The histogram showed the relative ratio of the expression levels of the target protein to that of an internal reference. (k) The mRNA expression of NLRP3 in lung tissues was analysed by qPCR. Representative results from three independent experiments are shown ($n = 3$). Scale bar, 20 μm . ns, not significant, * $p < 0.05$, ** $p < 0.01$, *** $p < 0.001$ (one-way ANOVA test; mean \pm SD).

by LPS + ATP (Figure S4F,G), which were similar to the results by the administration of M2 ϕ -EVs extracted by UC (Figure 3e-h). Thus, M2 ϕ -EVs extracted by different EV isolation methods exerted similar anti-inflammatory effect.

3.5 | M2 ϕ -EVs inhibited NLRP3 inflammasome activity via the NF- κ B pathway

Given the involvement of the NF- κ B pathway in the transcriptional regulation of NLRP3 (Zhao et al., 2019), we suspected that the inhibitory role of M2 ϕ -EV treatment on inflammasome activation might be linked to the NF- κ B signalling pathway suppression. As expected, the western blotting analysis demonstrated that M2 ϕ -EV treatment decreased the levels of phosphorylated p65 upon LPS + ATP stimulation (Figure 4a). And we also found that treatment with M2 ϕ -EVs significantly inhibited the nuclear translocation of p65, implying the blocked activity of the NF- κ B signalling pathway (Figure 4b).

Doxifluride, an activator of the NF- κ B signalling pathway, was used to further verify the regulatory role of the NF- κ B pathway in the NLRP3 inflammasome activity in response to M2 ϕ -EV treatment. We found that Doxifluride effectively activated the NF- κ B signalling pathway (Figure 4c) and substantially reduced the suppressive effect of M2 ϕ -EVs on the increased expression levels of NLRP3 protein and mRNA (Figure 4c,d) induced by LPS + ATP. These results suggested that M2 ϕ -EVs inhibited NLRP3 inflammasome activity by suppressing the NF- κ B signalling pathway in MH-S cells.

3.6 | miR-709 as a candidate miRNA responsible for the effect of M2 ϕ -EVs

In an effort to clarify whether miRNAs are a key mediator for the anti-inflammatory effect of M2 ϕ -EVs in LPS-induced ALI, miRNA-depleted M2 ϕ -EVs (M2 ϕ -EVs^{Dicer siRNA}) were generated via siRNA knockdown of Dicer, an essential polymerase required for miRNA synthesis, in M2-polarised MH-S cells (Figure 5a,b). Then we treated MH-S cells stimulated by LPS + ATP with M2 ϕ -EVs, M2 ϕ -EVs^{NC siRNA} and M2 ϕ -EVs^{Dicer siRNA} respectively. We found that miRNA depletion significantly weakened the inhibitory effect of M2 ϕ -EVs on the activation of the NF- κ B signalling pathway (Figure 5c), the subsequent cytokines release, including IL-6, TNF- α and IL-1 β (Figure 5d,e), and the elevated protein and mRNA expression levels of NLRP3 induced by LPS + ATP (Figure 5f,g). These results suggested that miRNAs within M2 ϕ -EVs contributed to their anti-inflammatory effect.

Next, we explored the specific miRNAs accountable for driving the main anti-inflammatory effect of M2 ϕ -EVs. M0 ϕ -EVs and M2 ϕ -EVs were sequenced to identify potentially efficient miRNAs, as the lack of protective effect exhibited by M0 ϕ -EVs in both in vivo (Figure S5A-C) and in vitro experiments (Figure S5D,E). The Venn diagram showed the shared and unique miRNAs between M0 ϕ -EVs and M2 ϕ -EVs (Figure 6a). Meanwhile, the scatter plot of all expressed miRNAs provided a clear visualisation of the differences in miRNA expression (Figure 6b). We then screened out 80 differentially expressed miRNAs (DE-miRNAs) by setting $|\text{Log}_2(\text{fold change})| > 1$ and p -value < 0.05 as the screening threshold (Figure 6c,d), of which 33 were downregulated and 47 were upregulated.

Then, we utilised TargetScan and miRanda databases to predict the target genes for all DE-miRNAs, with a specific focus on the 47 upregulated DE-miRNAs, which collectively had 17,427 target genes in both databases. GO and KEGG analyses were used to assess the potential functions of these upregulated DE-miRNAs based on their target genes. GO analysis revealed 7449 significantly enriched GO terms, encompassing 5779 biological processes, 606 cellular components and 1044 molecular functions involving immune response-regulating signalling pathway, receptor complex and protein serine/threonine kinase activity (Figure 6e). At the same time, 236 significantly enriched pathways were obtained by KEGG analysis, mainly involving in PI3K/Akt signalling pathway, MAPK signalling pathway and cytokine-cytokine receptor interaction, etc. (Figure 6f). Among them, the NOD-like receptor signalling pathway and NF- κ B signalling pathway were enriched, in agreement with our previous findings. These results indicated that M2 ϕ -EVs may regulate the NF- κ B/NLRP3 signalling pathway via these miRNAs to exert the anti-inflammatory effect.

To further identify the candidate miRNAs that mediated the protective effect of M2 ϕ -EVs, a comprehensive analysis of scatter plot, volcano plot and heatmap (Figure 6b-d) ultimately identified the top 7 upregulated DE-miRNAs with abundant expression, large fold change and high statistical significance (miR-5107-5p, miR-511-3p, miR-709, miR-378d, miR-125b-2-3p, miR-682-3p and miR-350-5p). qPCR confirmed that all of these 7 miRNAs were upregulated to varying degrees in M2 ϕ -EVs compared to M0 ϕ -EVs, consistent with the results of miRNA-sequencing analysis (Figure 6g).

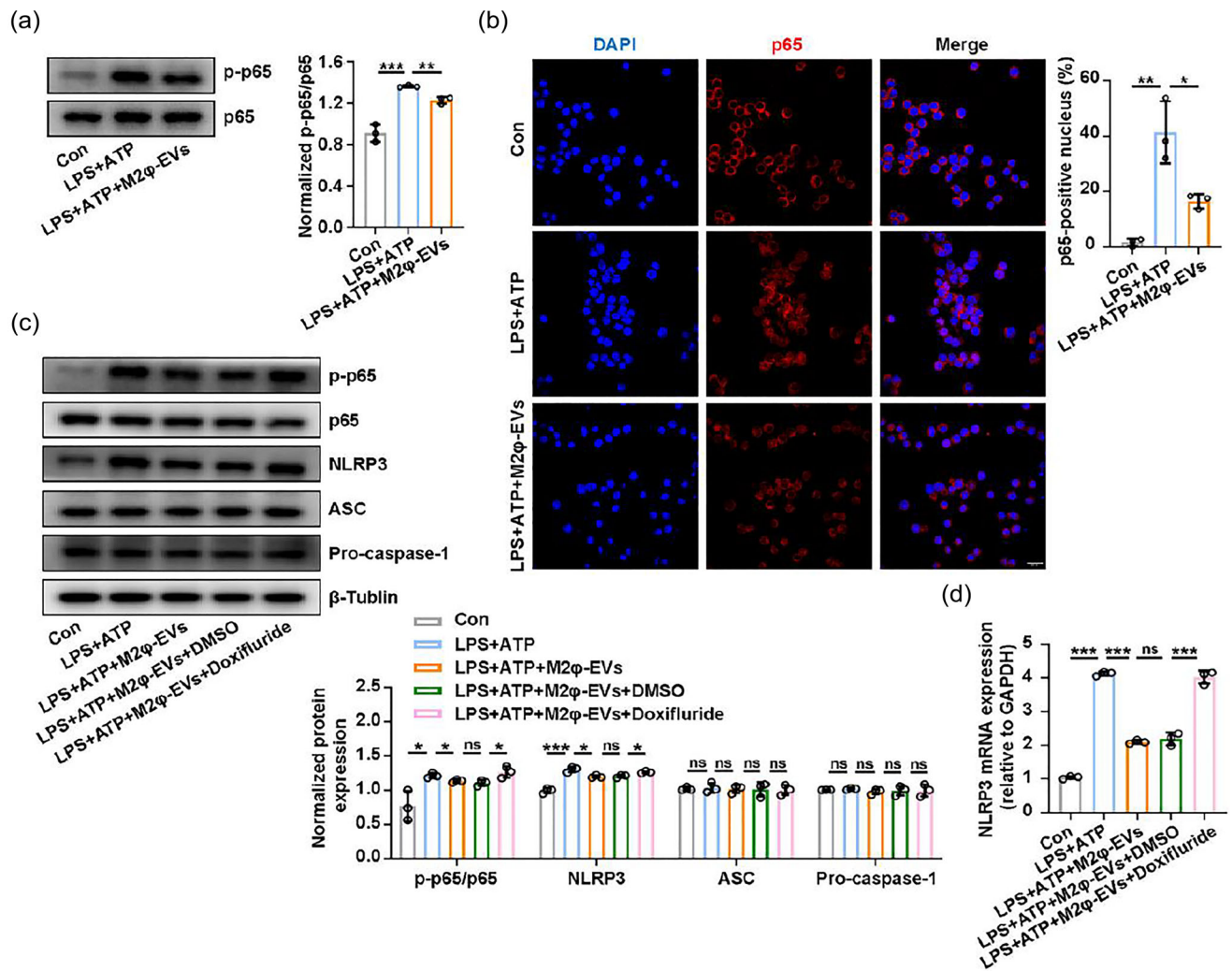


FIGURE 4 M2φ-EVs inhibited the NF-κB/NLRP3 inflammasome pathway. (a and b) After stimulation with LPS (0.5 μg/mL) for 30 min, MH-S cells were treated with M2φ-EVs (10 μg/mL) for 23 h and then subjected to ATP (0.5 mM) for another 30 min. (a) Western blotting analysis for phosphorylation levels of p65 in MH-S cells. The histogram showed the relative ratio of the expression levels of the target protein to that of an internal reference. (b) Nuclear localisation of p65 was visualised by immunofluorescence analysis in MH-S cells. The histogram represented the percentage of the p65 positive nucleus. (c and d) Pretreated with Doxifluride (10 mM) for 1 h, MH-S cells were then stimulated with LPS (0.5 μg/mL) for 30 min and then treated with M2φ-EVs (10 μg/mL) for 23 h and then subjected to ATP (0.5 mM) for another 30 min. (c) Western blotting analysis of p65, p-p65, NLRP3, ASC and Pro-caspase-1 levels in MH-S cells. The histogram showed the relative ratio of the expression levels of the target protein to that of an internal reference. (d) The mRNA expression of NLRP3 in MH-S cells was analysed by qPCR. Representative results from three independent experiments are shown ($n = 3$). Scale bar, 20 μm. ns, not significant, * $p < 0.05$, ** $p < 0.01$, *** $p < 0.001$ (one-way ANOVA test; mean \pm SD).

Based on the qPCR results, the top 4 DE-miRNAs (miR-5107-5p, miR-125b-2-3p, miR-709 and miR-350-5p) were selected for further testing. Only miR-709 was significantly upregulated in MH-S cells co-cultured with M2φ-EVs (Figure 6h), and this upregulation occurred in a concentration-dependent manner (Figure 6i). To further determine whether the elevated miR-709 levels in MH-S cells were a direct consequence of being shuttled from M2φ-EVs, we transiently transfected M2-polarised MH-S cells with miR-709 or FAM-labelled miR-709 respectively. Then, the conditioned culture medium from the cells mentioned above was collected to isolate and purify two different types of EVs. These purified EVs were then added to the culture medium of the initial MH-S cells, and FAM-labelled signals detected by confocal microscopy were only observed in MH-S cells incubated with FAM-labelled miR-709-M2φ-EVs but not with miR-709-M2φ-EVs (Figure 6j). In summary, these data suggested that M2φ-EVs mediated miR-709 shuttling.

3.7 | miR-709 mediated the protective effect of M2φ-EVs in vitro and in vivo

To determine the role of miR-709 in the anti-inflammatory effect of M2φ-EVs, we initially used miR-709 mimics and found that they effectively inhibited the activation of the NF-κB signalling pathway (Figure S6A), the release of cytokines IL-6, TNF-α and

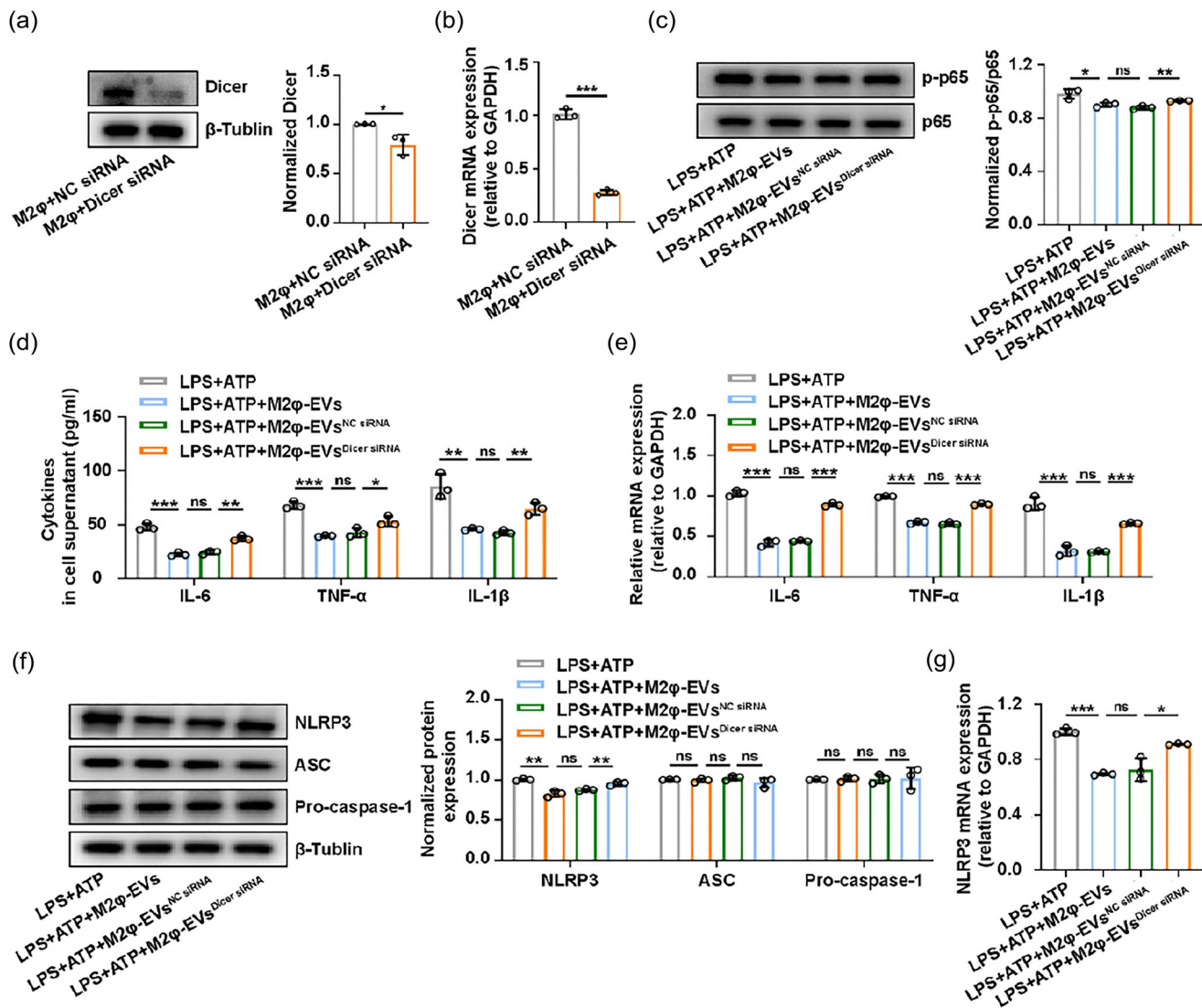


FIGURE 5 The biological effect of M2φ-EVs was partly mediated by miRNAs. (a and b) The MH-S cells treated with IL-4 were transfected with NC siRNA or Dicer siRNA for 24 h. (a) Western blotting analysis of Dicer levels in MH-S cells. The histogram showed the relative ratio of the expression levels of the target protein to that of an internal reference. (b) The mRNA of Dicer was detected by qPCR in MH-S cells. (c–g) The MH-S cells were stimulated with LPS (0.5 μg/mL) for 30 min and then treated with M2φ-EVs, M2φ-EVs^{NC siRNA} or M2φ-EVs^{Dicer siRNA} (10 μg/mL) respectively for 23 h and then subjected to ATP (0.5 mM) for another 30 min. (c) Western blotting analysis of phosphorylation levels of p65 in MH-S cells. The histogram showed the relative ratio of the expression levels of the target protein to that of an internal reference. (d) The concentrations of IL-6, TNF-α and IL-1β were measured by ELISA in cell supernatant. (e) The mRNA expressions of IL-6, TNF-α and IL-1β in MH-S cells were analysed by qPCR. (f) Western blotting analysis of NLRP3, ASC and Pro-caspase-1 levels in MH-S cells. The histogram showed the relative ratio of the expression levels of the target protein to that of an internal reference. (g) The mRNA expression of NLRP3 in MH-S cells was analysed by qPCR. Representative results from three independent experiments are shown ($n = 3$). ns, not significant, * $p < 0.05$, ** $p < 0.01$, *** $p < 0.001$ (one-way ANOVA test excepted for unpaired Student t -test in a, b; mean \pm SD).

IL-1β (Figure S6B,C), and the increased protein and mRNA expression levels of NLRP3 (Figure S6D,E) in MH-S cells induced by LPS + ATP. To further elucidate the regulatory effect of M2φ-EVs through miR-709, M2-polarised MH-S cells were transfected with miR-709 inhibitors or NC inhibitors (Figure 7a) to generate miR-709 inhibitor-M2φ-EVs and NC inhibitor-M2φ-EVs for in vitro validation (Figure 7b). As expected, miR-709 inhibitor-M2φ-EV treatment counteracted the anti-inflammatory effect of M2φ-EVs as evidenced by increases in the expression of p-p65 (Figure 7c), the secretion of IL-6, TNF-α and IL-1β (Figure 7d,e), and the expression levels of NLRP3 protein and mRNA (Figure 7f,g) in comparison with M2φ-EV treatment or NC inhibitor-M2φ-EV treatment.

To validate these in vitro findings, we subsequently conducted in vivo experiments to investigate whether the therapeutic effect of M2φ-EVs on ALI could be partly abolished by introducing miR-709 inhibitors. As shown in Figure 8a–c, the pathological alterations in lung tissues, the protein and inflammatory cytokines in BALF from LPS-induced ALI mice could not be significantly attenuated by miR-709 inhibitor-M2φ-EV administration. In addition, the downregulated levels of alveolar macrophages and

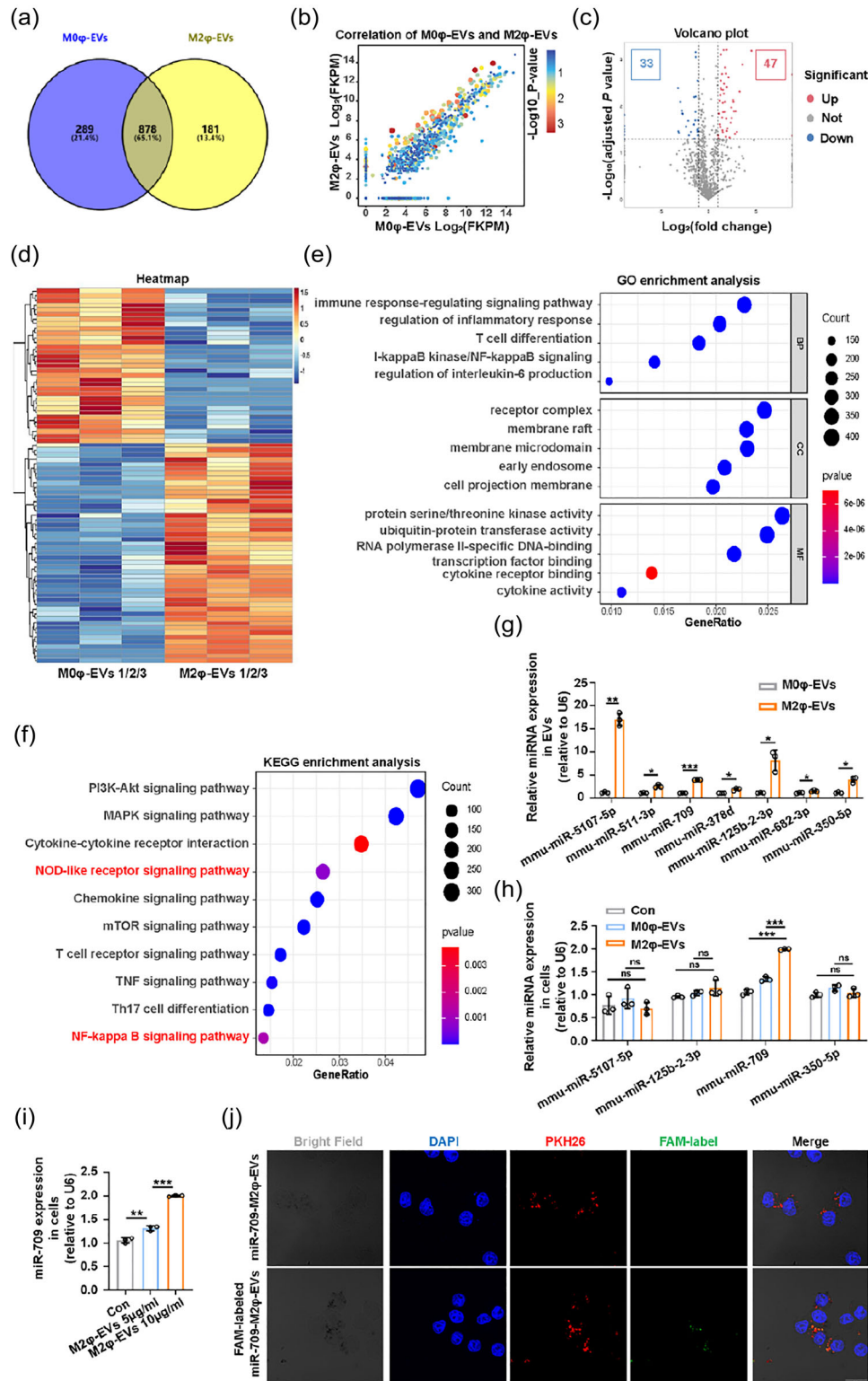


FIGURE 6 The identification of potentially effective candidate miRNAs in M2φ-EVs. (a) The Venn diagram of the shared and differential miRNAs in M0φ-EVs and M2φ-EVs. (b) The scatter plot of all expressed miRNAs in M0φ-EVs and M2φ-EVs. (c) The volcano map of all expressed miRNAs in M0φ-EVs and M2φ-EVs. (d) The heatmap of the 80 DE-miRNAs in M0φ-EVs and M2φ-EVs. (e) The GO enrichment analysis of the target genes of the 47 upregulated DE-miRNAs. (f) The KEGG enrichment analysis of the target genes of the 47 upregulated DE-miRNAs. (g) qPCR detection of the expressions of the selected 7 miRNAs in M0φ-EVs and M2φ-EVs. (h) qPCR detection of the expressions of the selected 4 miRNAs in MH-S cells co-cultured with PBS, M0φ-EVs or M2φ-EVs, respectively, for 24 h. (i) qPCR detection of the expression of miR-709 in MH-S cells co-cultured with different concentrations of M2φ-EVs for 24 h. (j) The uptake of the FAM-labelled miR-709-M2φ-EVs or miR-709-M2φ-EVs was visualised by immunofluorescence analysis in MH-S cells after incubation for 24 h. Representative results from three independent experiments are shown ($n = 3$). Scale bar, 20 μm . ns, not significant, $*p < 0.05$, $**p < 0.01$, $***p < 0.001$ (unpaired Student t -test in G; one-way ANOVA test in h, i; mean \pm SD).

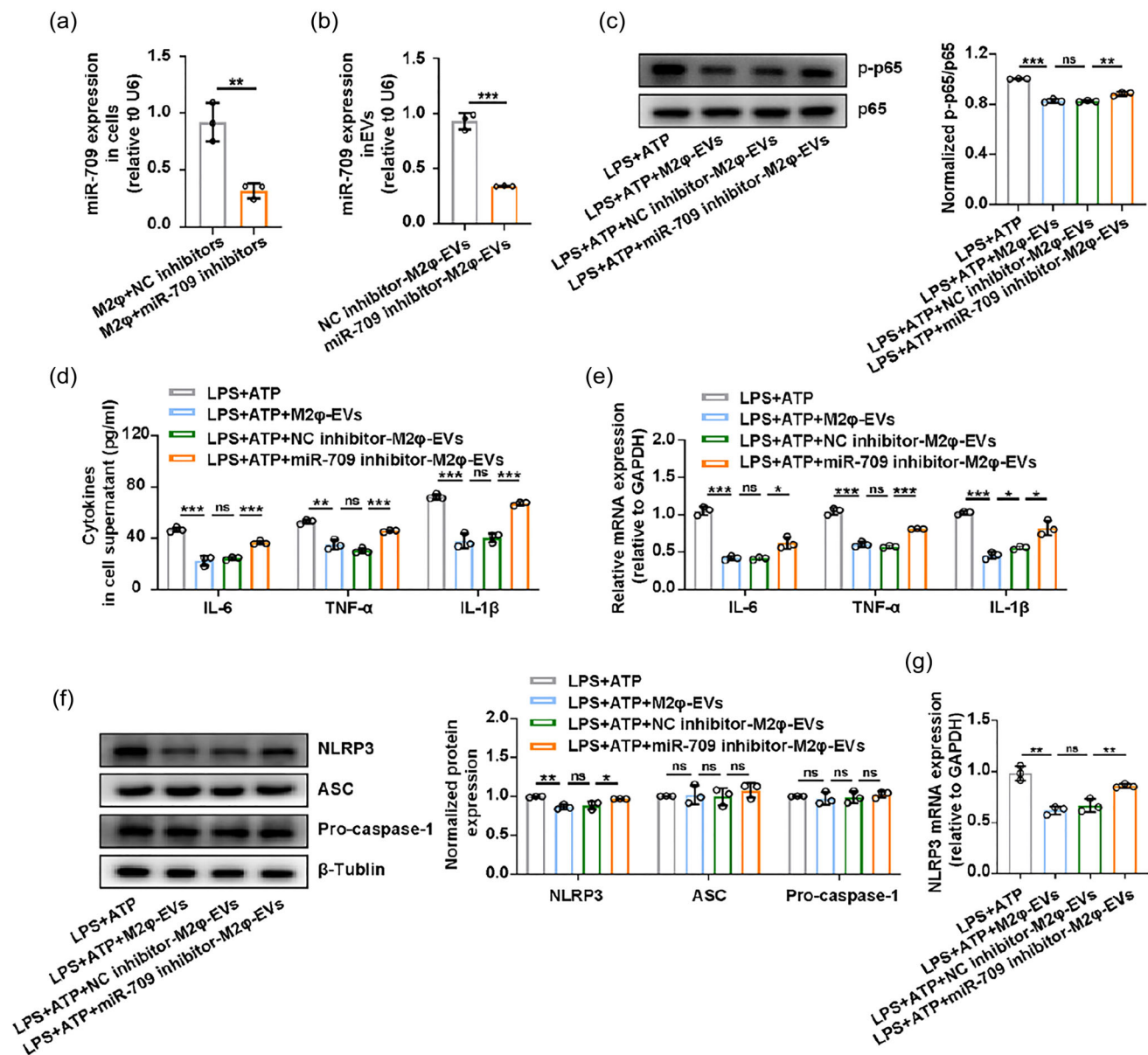


FIGURE 7 M2φ-EVs exerted the anti-inflammatory effect through miR-709 in vitro. (a and b) The MH-S cells were stimulated with IL-4 for 24 h and then transfected with NC inhibitors or miR-709 inhibitors for another 24 h. The expression of miR-709 was detected by qPCR in MH-S cells (a) or in NC inhibitor-M2φ-EVs and miR-709 inhibitor-M2φ-EVs (B). (c–g) MH-S cells were stimulated with LPS (0.5 μg/mL) for 30 min and then incubated with M2φ-EVs, NC inhibitor-M2φ-EVs or miR-709 inhibitor-M2φ-EVs for 23 h, and then subjected to ATP (0.5 mM) for another 30 min. (c) Western blotting analysis of p65 and p-p65 levels in the target protein to that of an internal reference. (d) The concentrations of IL-6, TNF-α and IL-1β in cell supernatant were measured by ELISA. (e) The mRNA expressions of IL-6, TNF-α and IL-1β in MH-S cells were analysed by qPCR. (f) Western blotting analysis of NLRP3, ASC and Pro-caspase-1 levels in MH-S cells. The histogram showed the relative ratio of the expression levels of the target protein to that of an internal reference. (g) The mRNA expression of NLRP3 in MH-S cells was analysed by qPCR. Representative results from three independent experiments are shown ($n = 3$). ns, not significant, $*p < 0.05$, $**p < 0.01$, $***p < 0.001$ (one-way ANOVA test excepted for unpaired Student t -test in a, b; mean \pm SD).

increased number of neutrophils in BALF caused by LPS were not reversed obviously in the miR-709 inhibitor-M2φ-EV administration group as compared to those in the M2φ-EV administration group or NC inhibitor-M2φ-EV administration group (Figure 8d,e). However, although the anti-inflammatory effect of M2φ-EVs was weakened after miR-709 elimination, several inflammatory indicators were still decreased to a different extent when treated with miR-709 inhibitor-M2φ-EVs, compared to the LPS/LPS + ATP group. These data suggested that miR-709 played a partial role in the anti-inflammatory effect of M2φ-EVs both in vivo and in vitro.

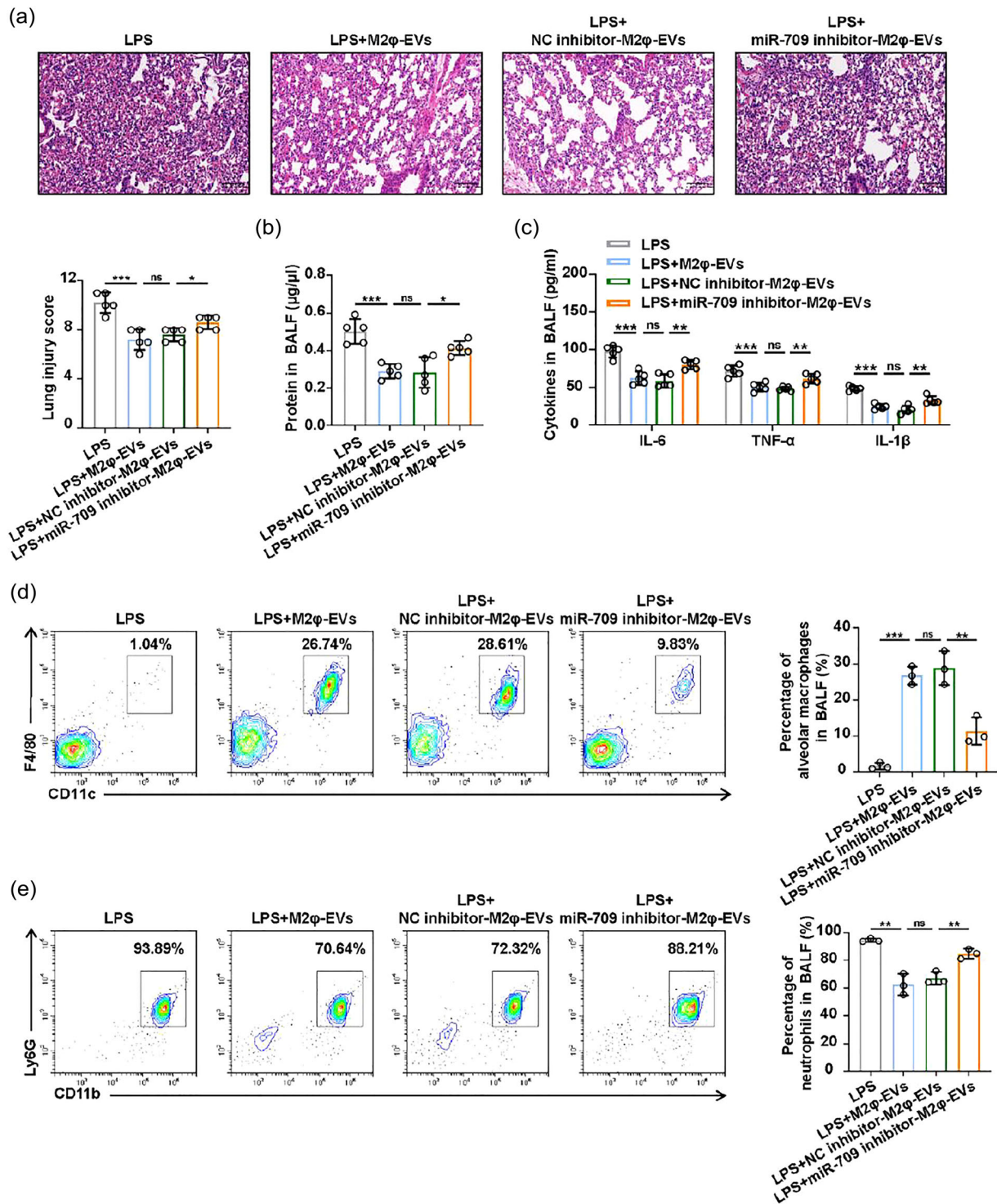


FIGURE 8 The protective effect of M2φ-EVs was mediated by miR-709 in vivo. C57BL/6 mice were pretreated with 1 mg/kg LPS intratracheally for 30 min, and then 100 μg M2φ-EVs, NC inhibitor-M2φ-EVs or miR-709 inhibitor-M2φ-EVs were injected intratracheally. These mice were sacrificed 24 h after LPS administration for the following experiments. (a) Representative H&E staining of lung tissues and the histogram showed the lung tissue pathological damage score. (b) The total protein concentration in BALF was detected by the BCA protein assay. (c) The concentrations of IL-6, TNF-α and IL-1β in BALF were measured by ELISA. (d and e) Flow cytometry analysis of alveolar macrophages (d) and neutrophils (e) in BALF. Representative results from three independent experiments are shown ($n = 5$ except for $n = 3$ in d, e). Scale bar, 100 μm. ns, not significant, $*p < 0.05$, $**p < 0.01$, $***p < 0.001$ (one-way ANOVA test; mean ± SD).

3.8 | miR-709 levels in BALF-EVs correlated with ALI/ARDS severity

To clinically confirm our findings, we first clarified whether miR-709 had a similar anti-inflammatory effect in human cell lines. We selected the THP-1 cells, a type of human monocyte, and found that miR-709 mimics could also inhibit the phosphorylation of p65 (Figure S7A), the release of cytokines IL-6, TNF- α and IL-1 β (Figure S7B–C), and the increased protein and mRNA expression levels of NLRP3 induced by LPS + ATP stimulation in THP-1 cells (Figure S7D,E). Given the anti-inflammatory effect of miR-709 in THP-1 cells, we further analysed whether miR-709 was also overexpressed in EVs derived from human M2 macrophages. In vitro polarisation of THP-1 cells was induced by IL-4, leading to increased expressions of M2-related markers CD206 and DC-SIGN (Figure S8A–C). Then, EVs were extracted from the culture supernatant of the initial THP-1 cells (T-M0 φ) and M2-like THP-1 cells (T-M2 φ), and were further characterised as T-M0 φ -EVs and T-M2 φ -EVs, showing cup-shaped vesicles in TEM (Figure S8D), with sizes of 162.4 and 153.6 nm respectively (Figure S8E). Among them, T-M2 φ -EVs exhibited increased CD206 expression, but the DC-SIGN was not detected in the vesicles (Figure S8F). qPCR analysis of M2-polarised THP-1 cells and their derived EVs revealed that both T-M2 φ (Figure S8G) and T-M2 φ -EVs (Figure S8H) highly expressed miR-709, indicating that the expression of miR-709 in T-M2 φ -EVs was similar to that in M2 φ -EVs, and it was reasonable to speculate that T-M2 φ -EVs might also exhibit the anti-inflammatory effect.

Indeed, T-M2 φ -EVs inhibited the release of cytokines IL-6, TNF- α and IL-1 β (Figure S8I,J) induced by LPS + ATP stimulation in THP-1 cells. Additionally, considering that the EVs we previously used were derived from cell lines of human and mice, and it is unclear whether similar phenomena could be observed in EVs derived from primary cells. To address this, we first extracted mouse primary peritoneal macrophages (MP-M φ) and human primary CD14⁺ monocytes (HP-M φ), and then induced the initial MP-M φ (MP-M0 φ) and HP-M φ (HP-M0 φ) to M2 polarisation (MP-M2 φ , HP-M2 φ) (Figures S9A,B and S10A,B). Further collected EVs from MP-M0 φ , MP-M2 φ , HP-M0 φ and HP-M2 φ were characterised and termed as MP-M0 φ -EVs, MP-M2 φ -EVs, HP-M0 φ -EVs and HP-M2 φ -EVs, respectively (Figures S9C–E and S10C–E). As expected, the expression of miR-709 was also elevated in both MP-M2 φ and MP-M2 φ -EVs (Figure S9F,G), and a similar elevation was observed in HP-M2 φ and HP-M2 φ -EVs (Figure S10F,G). Moreover, the application of MP-M2 φ -EVs effectively down-regulated the release of IL-6, TNF- α and IL-1 β in LPS+ATP induced MP-M φ (Figure S9I,J). Likewise, HP-M2 φ -EVs exerted a similar role in HP-M φ stimulated by LPS+ATP (Figure S10I,J). These results indicated that the M2 polarisation of human or mouse macrophages can promote the expression of miR-709, whether in cell lines or primary cells. However, extra experimental verification is needed to further determine whether the anti-inflammatory effect of T-M2 φ -EVs, MP-M2 φ -EVs and HP-M2 φ -EVs is mediated by miR-709.

Finally, to understand the relationship between miR-709 expression and disease progression, we first detected the miR-709 expression in BALF-EVs of mice at 6 and 24 h after LPS administration. The results showed that the expression of miR-709 was significantly downregulated as ALI progressed in mice (Figure 9a). In clinical samples, miR-709 expression in the collected BALF-EVs (Figure 9b) was lower in ARDS patients compared to the control group (Figure 9c). Meanwhile, a simple linear regression analysis was conducted between the expression of miR-709 in BALF-EVs of ARDS patients and their PaO₂/FiO₂, Murray score, SOFA score, duration of mechanical ventilation, and hospital length of stay. We found that miR-709 expression in BALF-EVs was positively correlated with the PaO₂/FiO₂, negatively correlated with the Murray score, and had no significant correlation with the remaining three indicators (Figure 9d). These results suggested that miR-709 was also present in human M2 φ -EVs, and might potentially serve as a valuable biomarker to indicate the severity of lung injury in ARDS patients.

4 | DISCUSSION

The present study demonstrated that the implementation of M2 φ -EVs effectively alleviated LPS-induced ALI and clarified the underlying mechanism. We have successfully associated specific experimental findings with clinical relevance, as a correlation was discovered between the components responsible for the anti-inflammatory effect of M2 φ -EVs and the disease severity in ARDS patients (Figure 10).

In recent years, the pivotal role of alveolar macrophage polarisation in controlling inflammatory lung diseases has gained recognition (Feng et al., 2023; Song et al., 2019). Therefore, numerous studies have focused on modulating the polarisation of macrophages, particularly with the goal of increasing the proportion of M2-like alveolar macrophages to manage ALI/ARDS (Feng et al., 2023; Song et al., 2019). However, little attention has been paid to the changes in the polarisation ratio of AM-EVs within the body, despite substantial evidence suggesting that macrophage-derived EVs are pivotal components for their in vivo functionality. The present study was the first to demonstrate that as ALI progressed, the ratio of M2/M1-like AM-EVs initially declined significantly, mirroring the changes in the M2/M1-like alveolar macrophage populations, suggesting that shifting the focus from alveolar macrophages to their EVs might offer an innovative therapeutic strategy.

Recent studies have reported that the levels of proinflammatory cytokines (TNF- α , IL-1 β and IL-6) were elevated in AM-EVs from ALI mice, with TNF- α being particularly prominent, which is consistent with our research, indicating an increased proportion of M1-like AM-EVs in ALI (Soni et al., 2016; Wang et al., 2022). Further investigation revealed that these AM-EVs could activate inflammation-related signalling pathways, leading to oxidative stress damage and worsening of LPS-induced ALI (Wang et al., 2022). However, the role of AM-EVs elaborated here was mainly focused on their overall effect, whilst the specific

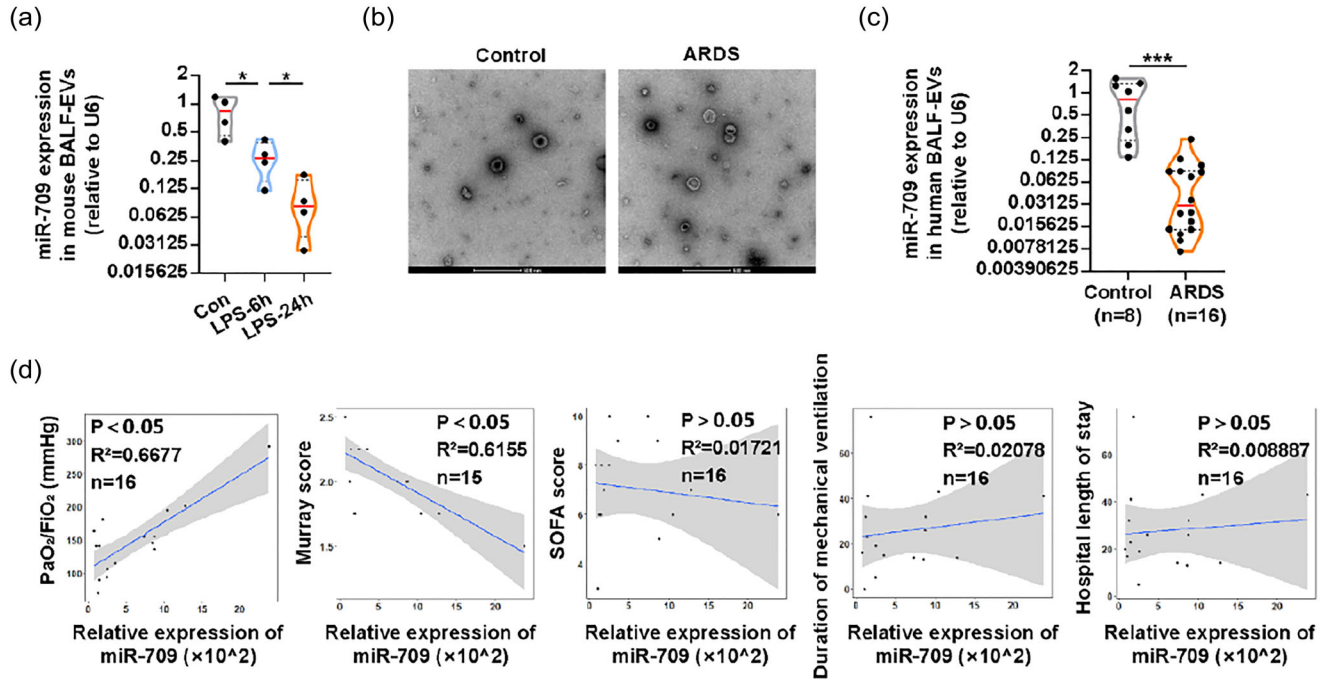


FIGURE 9 miR-709 expression in BALF-EVs was correlated with the severity of ALI/ARDS. (a) The relative expression of miR-709 in BALF-EVs of mice at different time points after LPS administration was detected by qPCR. (b) Representative TEM images of BALF-EVs of control and ARDS patients. (c) The expression of miR-709 in BALF-EVs of control and ARDS patients was detected by qPCR. (d) The correlation between the levels of miR-709 in BALF-EVs of ARDS patients with their PaO₂/FiO₂, Murray score, SOFA score, duration of mechanical ventilation, and hospital length of stay. Representative results from three independent experiments are shown (*n* = 4 in a). Scale bar, 200 nm. **p* < 0.05, ****p* < 0.001 (one-way ANOVA test in a; unpaired Student *t*-test in c; Spearman rank-order correlation test in d; mean ± SD).

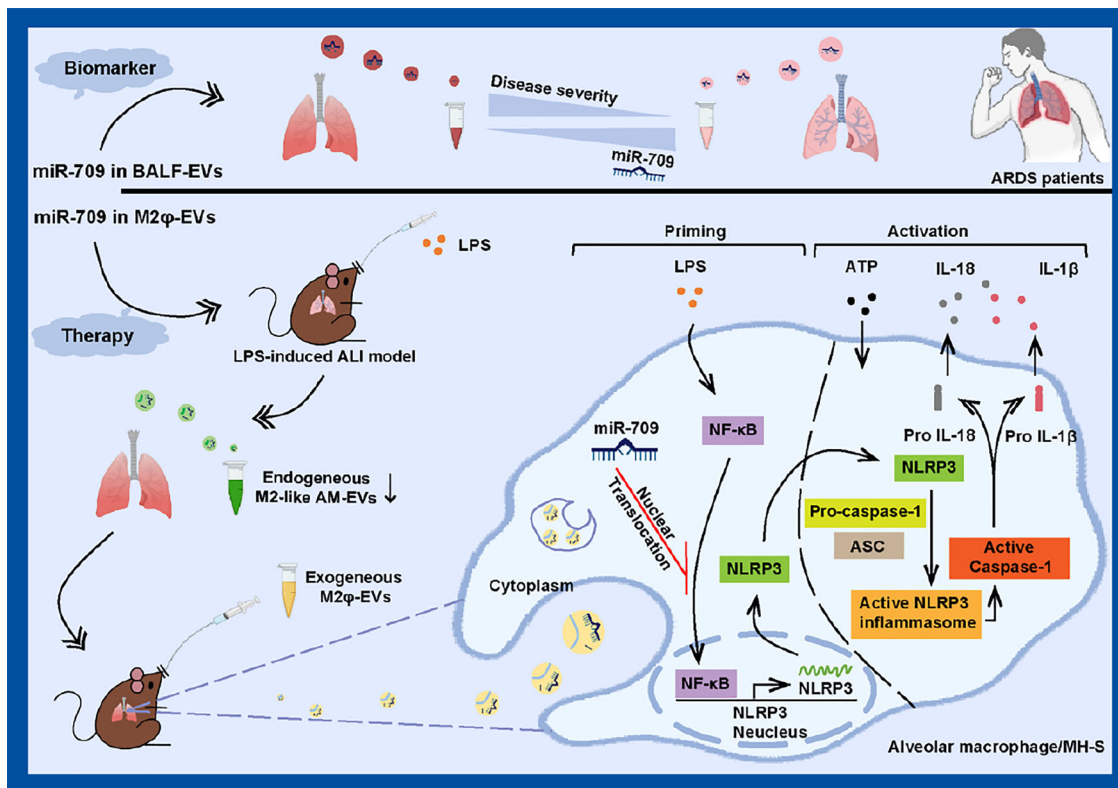


FIGURE 10 Schematic diagram of the potential role of M2φ-EVs on ALI/ARDS. Endogenous M2-like AM-EVs decreased in LPS-induced ALI mice model, whilst exogenous M2φ-EVs alleviated ALI progression primarily by transferring miR-709 through the NF-κB/NLRP3 inflammasome axis, with the potential of miR-709 as a biomarker for assessing ALI/ARDS severity.

effect of M2-like AM-EVs were rarely mentioned. As a result, there has been a growing interest in recent studies investigating the role of M2 ϕ -EVs. A previous study demonstrated that M2 ϕ -EVs protected against septic lung injury in mice (Mulcahy et al., 2014). Despite suggesting a protective role of M2 ϕ -EVs in lung injury, it is important to note that the M2 ϕ -EVs in that study were originated from peritoneal macrophages and the disease model employed was sepsis-related. In contrast, we mainly utilised the MH-S cell line, which closely resembled primary alveolar macrophages, allowing a more thorough exploration of the effect of endogenous M2-like AM-EVs. The development of the LPS-induced lung injury model also provided new avenues for exploring the therapeutic potential of M2 ϕ -EVs.

Thus, we introduced exogenous M2 ϕ -EVs into mice injected with PBS or LPS and found that they localised primarily to alveolar macrophages. We are not surprised by the fact that macrophages constitute the predominant cell subset responsible for the uptake of M2 ϕ -EVs, as numerous studies have shown that macrophages can regulate their uptake of EVs through various pathways, including macropinocytosis, endocytosis and phagocytosis, with phagocytosis being the main approach (Mulcahy et al., 2014). Further investigation unveiled the immune regulatory and lung protective effect of M2 ϕ -EVs in LPS-induced ALI, primarily attributed to the suppression of alveolar macrophage pyroptosis. Pyroptosis, a recently recognised form of programmed cell death in inflammatory cells, has been identified as a critical step in the development of ALI/ARDS, highlighting its potential significance as a therapeutic target for preventing and treating these conditions (De Nardo et al., 2014). Although it has been reported that the cytosolic transfer of LPS by EVs could lead to non-canonical activation of NLRP3 inflammasome and pyroptosis, this 'side effect' can be ignored in our experiment due to the weak binding ability of M2 ϕ -EVs and LPS.

It is well-established that EV-associated miRNAs can be delivered to target cells as functional cargo (Valadi et al., 2007). Our results suggested that miR-709, as a potent anti-inflammatory miRNA, was elevated to varying degrees in several types of M2 macrophage-derived EVs in both human and mice. Further investigation indicated that M2 ϕ -EVs could exert their protective role by transferring miR-709 to stressed alveolar macrophages. Conversely, the anti-inflammatory effect of M2 ϕ -EVs was reversed by the application of miR-709 inhibitors. Thus, miR-709 emerged as a functional molecule within M2 ϕ -EVs, crucial for attenuating LPS-induced lung inflammation. Previous studies have reported the key role of miR-709 in cell proliferation, migration and invasiveness, as well as modulation of cellular inflammatory response (Li et al., 2016; Liu et al., 2015). However, our study here, for the first time, reported that miR-709 in M2 ϕ -EVs served as an inhibitor of alveolar macrophage pyroptosis and lung inflammation in ALI/ARDS.

The mechanism through which M2 ϕ -EVs-derived miR-709 modulated the activation of NLRP3 inflammasome in alveolar macrophages was further investigated by demonstrating its repressive effect on the NF- κ B pathway. The data here showed a significant reduction of p-p65 in MH-S cells when treated with M2 ϕ -EVs. The administration of miR-709 inhibitors could remarkably weaken the M2 ϕ -EVs' suppressive effect on p-p65 and its downstream NLRP3 protein expression. Furthermore, it is notable that the application of M2 ϕ -EVs could decrease the release of cytokines both in vivo and in vitro, including the IL-1 β , as well as IL-6 and TNF- α , which two were independent of the activation of NLRP3 inflammasome, and the inhibition was reversed after the introduction of miR-709 inhibitor-M2 ϕ -EVs. Considering that the NF- κ B signalling pathway contributes to the induction of inflammatory chemokines (Hayden et al., 2008), and the observed inhibitory effect of M2 ϕ -EVs on the NF- κ B pathway may potentially explain the phenomenon of simultaneous downregulation of both inflammasome-dependent and -independent cytokine release by M2 ϕ -EVs. Overall, we suggested that M2 ϕ -EVs offer protection against LPS-induced ALI through the miR-709/NF- κ B/NLRP3 inflammasome axis.

Additionally, we found a gradual decline in miR-709 expression in BALF-EVs from ARDS patients, with a clear correlation with ARDS severity, as indicated by the PaO₂/FiO₂ and Murray score. However, the lack of a significant association between miR-709 levels and the SOFA score may be because the SOFA score encompasses multiple organ failure, and the specific functions of miR-709 within these organs remain poorly understood. Notably, there was no significant correlation between the expression of miR-709 in BALF-EVs and ARDS prognosis, which may be attributed to the clinical complexity of the overall prognosis of patients that cannot be entirely explained by a single factor. Nevertheless, these clinical data supported the conclusion that miR-709 contributed to inhibiting lung inflammation and might serve as a potential biomarker for ARDS severity.

However, the present study has certain limitations, offering avenues for future research. First, whilst we primarily used LPS as a representative stimulus for infectious ARDS, there are other infectious components such as bacterial lipoprotein, CpG-ODN, flagellin and respiratory viruses that were not explored. Expanding our research to investigate the effect of different stimuli on endogenous M2-like AM-EV reduction in the lungs and evaluating the therapeutic impact of exogenous M2 ϕ -EVs in various stimuli-induced ALI would be valuable. Second, although our study highlighted the role of miR-709 in the anti-inflammatory efficacy of M2 ϕ -EVs in LPS-induced ALI, further research is required to investigate the contributions of other contents such as proteins, DNA and mRNA to comprehensively assess the effect of M2 ϕ -EVs. Third, even though miR-709 is known to be a mouse-specific miRNA (Park et al., 2023), our study demonstrated that miR-709 is highly expressed in T-M2 ϕ , HP-M2 ϕ and their derived EVs, as well as in the BALF-EVs from clinical samples. Actually, similar findings have been observed for several other mouse-specific miRNAs, including miR-6238, miR-717 and miR-6240, in various human cells and tissues (Adamowicz et al., 2018; Guo et al., 2018; Hanousková et al., 2019; Huang et al., 2011; Kunej et al., 2010). Further experimental and clinical validation is necessary to ascertain whether these miRNAs have species-specificity. Finally, in our analysis of clinical samples, the sample size for both experimental and control groups was relatively small, and larger, multi-centre studies are needed to establish a robust correlation between miR-709 expression in BALF-EVs and ARDS severity.

In summary, our data indicated that endogenous M2-like AM-EVs are declined in LPS-induced ALI, and exogenous M2 ϕ -EVs alleviated the development of ALI primarily through inhibiting the NF- κ B/NLRP3 inflammasome axis via miR-709 transfer, with miR-709 showing potential as a suitable biomarker for assessing ALI/ARDS severity (Figure 10). These results provide a promising strategy to evaluate and treat ALI/ARDS via targeting M2 ϕ -EVs.

AUTHOR CONTRIBUTIONS

Jie Yang, Xiaofang Huang, Qing Yu, Shibo Wang, Xuehuan Wen, Songjie Bai, Lanxin Cao, Kai Zhang and Shufang Zhang performed various experiments; Gensheng Zhang, Zhijian Cai, Zhanghui Chen and Xingang Wang designed the project and supervised the study; Jie Yang and Gensheng Zhang wrote the manuscript.

ACKNOWLEDGEMENTS

This work was supported in part by grants from the National Natural Science Foundations of China (No. 82270086, No. 81971871, GS Zhang), the National Key Research and Development Program of China (2022YFC2403100, XG Wang), the National Natural Science Foundations of China (No. 81971886, No.82170053, ZH Chen), the Natural Science Foundation of Shandong Province (No. ZR202111020044, XF Huang) and the Key Research and Development Program of Zhejiang Province (No.2024C03186, YA Xu). And the authors would like to thank Dr. Yesong Wang, Yang Yu, Shujun Dai, Linlin Du and Hui Shan in the Department of Critical Care Medicine at the Second Affiliated Hospital of Zhejiang University for human sample collections.

CONFLICT OF INTEREST STATEMENT

The authors declare no competing interests.

DATA AVAILABILITY STATEMENT

All data needed to evaluate the conclusions in the paper are presented in the main manuscript and the Supplementary Information.

ORCID

Zhijian Cai  <https://orcid.org/0000-0003-4317-2630>

Gensheng Zhang  <https://orcid.org/0000-0001-9298-3961>

REFERENCES

- Adamowicz, M., Morgan, C. C., Haubner, B. J., Nosedá, M., Collins, M. J., Abreu Paiva, M., Srivastava, P. K., Gellert, P., Razzaghi, B., O'Gara, P., & Raina, P. (2018). Functionally conserved noncoding regulators of cardiomyocyte proliferation and regeneration in mouse and human. *Circulation Genomic and Precision Medicine*, 11, e01805.
- Aggarwal, N. R., King, L. S., & D'Alessio, F. R. (2014). Diverse macrophage populations mediate acute lung inflammation and resolution. *American Journal of Physiology Lung Cellular and Molecular Physiology*, 306, L709–L725.
- Atianand, M. K., Rathinam, V. A., & Fitzgerald, K. A. (2013). SnapShot: Inflammasomes. *Cell*, 153, 272–272.e271.
- Bai, L., Chen, Y., Zheng, S., Ren, F., Kong, M., Liu, S., Han, Y., & Duan, Z. (2019). Phenotypic switch of human and mouse macrophages and resultant effects on apoptosis resistance in hepatocytes. *Innate Immunity*, 25, 176–185.
- Bai, L., Fu, L., Li, L., Ren, F., Zheng, Q., Liu, S., Han, Y., Zheng, S., Chen, Y., & Duan, Z. (2018). Cellular mechanisms of hepatoprotection mediated by M2-like macrophages. *Medical Science Monitor: International Medical Journal of Experimental and Clinical Research*, 24, 2675–2682.
- Bai, L., Kong, M., Duan, Z., Liu, S., Zheng, S., & Chen, Y. (2021). M2-like macrophages exert hepatoprotection in acute-on-chronic liver failure through inhibiting necroptosis-S100A9-necroinflammation axis. *Cell Death & Disease*, 12, 93.
- Bai, L., Liu, X., Zheng, Q., Kong, M., Zhang, X., Hu, R., Lou, J., Ren, F., Chen, Y., Zheng, S., & Liu, S. (2017). M2-like macrophages in the fibrotic liver protect mice against lethal insults through conferring apoptosis resistance to hepatocytes. *Scientific Reports*, 7, 10518.
- De Nardo, D., De Nardo, C. M., & Latz, E. (2014). New insights into mechanisms controlling the NLRP3 inflammasome and its role in lung disease. *The American Journal of Pathology*, 184, 42–54.
- Feng, Z., Jing, Z., Li, Q., Chu, L., Jiang, Y., Zhang, X., Yan, L., Liu, Y., Jiang, J., Xu, P., & Chen, Q. (2023). Exosomal STIMATE derived from type II alveolar epithelial cells controls metabolic reprogramming of tissue-resident alveolar macrophages. *Theranostics*, 13, 991–1009.
- Guo, Y., Ni, J., Chen, S., Bai, M., Lin, J., Ding, G., Zhang, Y., Sun, P., Jia, Z., Huang, S., & Yang, L. (2018). MicroRNA-709 mediates acute tubular injury through effects on mitochondrial function. *Journal of the American Society of Nephrology: JASN*, 29, 449–461.
- Hanousková, B., Skála, M., Brynychová, V., Zárýbnický, T., Skarková, V., Kazimířová, P., Vernerová, A., Souček, P., Skálová, L., Pudil, R., & Matoušková, P. (2019). Imatinib-induced changes in the expression profile of microRNA in the plasma and heart of mice—A comparison with doxorubicin. *Biomedicine & Pharmacotherapy = Biomedecine & Pharmacotherapie*, 115, 108883.
- Hayden, M. S., & Ghosh, S. (2008). Shared principles in NF- κ B signaling. *Cell*, 132, 344–362.
- Hou, Y., Liu, Y., Liang, S., Ding, R., Mo, S., Yan, D., & Li, D. (2021). The novel target: Exosomes derived from M2 macrophage. *International Reviews of Immunology*, 40, 183–196.
- Huang, C., Du, W., Ni, Y., Lan, G., & Shi, G. (2022). The effect of short-chain fatty acids on M2 macrophages polarization in vitro and in vivo. *Clinical and Experimental Immunology*, 207, 53–64.
- Huang, W., Liu, H., Wang, T., Zhang, T., Kuang, J., Luo, Y., Chung, S. S., Yuan, L., & Yang, J. Y. (2011). Tonicity-responsive microRNAs contribute to the maximal induction of osmoregulatory transcription factor OREBP in response to high-NaCl hypertonicity. *Nucleic Acids Research*, 39, 475–485.
- Huang, X., Xiu, H., Zhang, S., & Zhang, G. (2018). The role of macrophages in the pathogenesis of ALI/ARDS. *Mediators of Inflammation*, 2018, 1264913.
- Jiang, L., Shen, Y., Guo, D., Yang, D., Liu, J., Fei, X., Yang, Y., Zhang, B., Lin, Z., Yang, F., & Wang, X. (2016). EpCAM-dependent extracellular vesicles from intestinal epithelial cells maintain intestinal tract immune balance. *Nature Communications*, 7, 13045.

- Kulikauskaitė, J., & Wack, A. (2020). Teaching old dogs new tricks? The plasticity of lung alveolar macrophage subsets. *Trends in Immunology*, *41*, 864–877.
- Kumari, P., Vasudevan, S. O., Russo, A. J., Wright, S. S., Fraile-Ágreda, V., Krajewski, D., Jellison, E. R., Rubio, I., Bauer, M., Shimoyama, A., & Fukase, K. (2023). Host extracellular vesicles confer cytosolic access to systemic LPS licensing non-canonical inflammasome sensing and pyroptosis. *Nature Cell Biology*, *25*, 1860–1872.
- Kunej, T., Skok, D. J., Horvat, S., Dovc, P., & Jiang, Z. (2010). The glypican 3-hosted murine mir717 gene: Sequence conservation, seed region polymorphisms and putative targets. *International Journal of Biological Sciences*, *6*, 769–772.
- Li, M., Chen, H., Chen, L., Chen, Y., Liu, X., & Mo, D. (2016). miR-709 modulates LPS-induced inflammatory response through targeting GSK-3 β . *International Immunopharmacology*, *36*, 333–338.
- Lin, Y., Yang, X., Yue, W., Xu, X., Li, B., Zou, L., & He, R. (2014). Chemerin aggravates DSS-induced colitis by suppressing M2 macrophage polarization. *Cellular & Molecular Immunology*, *11*, 355–366.
- Liu, H., He, Y., Lu, C., Zhang, P., Zhou, C., Ni, Y., Niu, W., Yuan, X., Li, P., Zheng, J., & Qin, Y. (2019). Efficacy of pulmonary transplantation of engineered macrophages secreting IL-4 on acute lung injury in C57BL/6 mice. *Cell Death & Disease*, *10*, 664.
- Liu, T., Zhang, X., Sha, K., Liu, X., Zhang, L., & Wang, B. (2015). miR-709 up-regulated in hepatocellular carcinoma, promotes proliferation and invasion by targeting GPC5. *Cell Proliferation*, *48*, 330–337.
- Lou, P., Liu, S., Xu, X., Pan, C., Lu, Y., & Liu, J. (2021). Extracellular vesicle-based therapeutics for the regeneration of chronic wounds: Current knowledge and future perspectives. *Acta Biomaterialia*, *119*, 42–56.
- Mao, R., Wang, C., Zhang, F., Zhao, M., Liu, S., Liao, G., Li, L., Chen, Y., Cheng, J., Liu, J., & Lu, Y. (2020). Peritoneal M2 macrophage transplantation as a potential cell therapy for enhancing renal repair in acute kidney injury. *Journal of Cellular and Molecular Medicine*, *24*, 3314–3327.
- Mulcahy, L. A., Pink, R. C., & Carter, D. R. (2014). Routes and mechanisms of extracellular vesicle uptake. *Journal of Extracellular Vesicles*, *3*(1), 24641.
- Park, S., Kim, M., Park, M., Jin, Y., Lee, S. J., & Lee, H. (2023). Specific upregulation of extracellular miR-6238 in particulate matter-induced acute lung injury and its immunomodulation. *Journal of Hazardous Materials*, *445*, 130466.
- Ranieri, V. M., Rubenfeld, G. D., Thompson, B. T., Ferguson, N. D., Caldwell, E., Fan, E., Camporota, L., & Slutsky, A. S. (2012). Acute respiratory distress syndrome: The Berlin definition. *JAMA*, *307*, 2526–2533.
- Rubenfeld, G. D., Caldwell, E., Peabody, E., Weaver, J., Martin, D. P., Neff, M., Stern, E. J., & Hudson, L. D. (2005). Incidence and outcomes of acute lung injury. *The New England Journal of Medicine*, *353*, 1685–1693.
- Song, C., Li, H., Li, Y., Dai, M., Zhang, L., Liu, S., Tan, H., Deng, P., Liu, J., Mao, Z., & Li, Q. (2019). NETs promote ALI/ARDS inflammation by regulating alveolar macrophage polarization. *Experimental Cell Research*, *382*, 111486.
- Song, H., Liu, B., Huai, W., Yu, Z., Wang, W., Zhao, J., Han, L., Jiang, G., Zhang, L., Gao, C., & Zhao, W. (2016). The E3 ubiquitin ligase TRIM31 attenuates NLRP3 inflammasome activation by promoting proteasomal degradation of NLRP3. *Nature Communications*, *7*(1), 13727.
- Song, H., Zhao, C., Yu, Z., Li, Q., Yan, R., Qin, Y., Jia, M., & Zhao, W. (2020). UAF1 deubiquitinase complexes facilitate NLRP3 inflammasome activation by promoting NLRP3 expression. *Nature Communications*, *11*(1), 6042.
- Soni, S., Wilson, M. R., O’Dea, K. P., Yoshida, M., Katbeh, U., Woods, S. J., & Takata, M. (2016). Alveolar macrophage-derived microvesicles mediate acute lung injury. *Thorax*, *71*, 1020–1029.
- Tang, T. T., Wang, B., Wu, M., Li, Z. L., Feng, Y., Cao, J. Y., Yin, D., Liu, H., Tang, R. N., Crowley, S. D., & Lv, L. L. (2020). Extracellular vesicle-encapsulated IL-10 as novel nanotherapeutics against ischemic AKI. *Science Advances*, *6*, eaaz0748.
- Valadi, H., Ekström, K., Bossios, A., Sjöstrand, M., Lee, J. J., & Lötvall, J. O. (2007). Exosome-mediated transfer of mRNAs and microRNAs is a novel mechanism of genetic exchange between cells. *Nature Cell Biology*, *9*, 654–659.
- Wang, W., Zhu, L., Li, H., Ren, W., Zhuo, R., Feng, C., He, Y., Hu, Y., & Ye, C. (2022). Alveolar macrophage-derived exosomal tRF-22-8BWS7K092 activates Hippo signaling pathway to induce ferroptosis in acute lung injury. *International Immunopharmacology*, *107*, 108690.
- Wang, Y., Zhao, M., Liu, S., Guo, J., Lu, Y., Cheng, J., & Liu, J. (2020). Macrophage-derived extracellular vesicles: Diverse mediators of pathology and therapeutics in multiple diseases. *Cell Death & Disease*, *11*, 924.
- Watanabe, Y., Tsuchiya, A., & Terai, S. (2021). The development of mesenchymal stem cell therapy in the present, and the perspective of cell-free therapy in the future. *Clinical and Molecular Hepatology*, *27*, 70–80.
- Xia, L., Zhang, C., Lv, N., Liang, Z., Ma, T., Cheng, H., Xia, Y., & Shi, L. (2022). AdMSC-derived exosomes alleviate acute lung injury via transferring mitochondrial component to improve homeostasis of alveolar macrophages. *Theranostics*, *12*, 2928–2947.
- Xiu, H., Peng, Y., Huang, X., Gong, J., Yang, J., Cai, J., Zhang, K., Cui, W., Shen, Y., Wang, J., & Zhang, S. (2023). Neddylation alleviates methicillin-resistant staphylococcus aureus infection by inducing macrophage reactive oxygen species production. *Journal of Immunology (Baltimore, Md : 1950)*, *207*, 296–307.
- Yang, H., Lv, H., Li, H., Ci, X., & Peng, L. (2019). Oridonin protects LPS-induced acute lung injury by modulating Nrf2-mediated oxidative stress and Nrf2-independent NLRP3 and NF- κ B pathways. *Cell Communication and Signaling : CCS*, *17*, 62.
- Yang, J., Yang, J., Huang, X., Xiu, H., Bai, S., Li, J., Cai, Z., Chen, Z., Zhang, S., & Zhang, G. (2022). Glibenclamide alleviates LPS-induced acute lung injury through NLRP3 inflammasome signaling pathway. *Mediators of Inflammation*, *2022*, 8457010.
- Zhang, G., Huang, X., Xiu, H., Sun, Y., Chen, J., Cheng, G., Song, Z., Peng, Y., Shen, Y., Wang, J., & Cai, Z. (2020). Extracellular vesicles: Natural liver-accumulating drug delivery vehicles for the treatment of liver diseases. *Journal of Extracellular Vesicles*, *10*, e12030.
- Zhao, W., Ma, L., Cai, C., & Gong, X. (2019). Caffeine inhibits NLRP3 inflammasome activation by suppressing MAPK/NF- κ B and A2aR signaling in LPS-induced THP-1 macrophages. *International Journal of Biological Sciences*, *15*, 1571–1581.

SUPPORTING INFORMATION

Additional supporting information can be found online in the Supporting Information section at the end of this article.

How to cite this article: Yang, J., Huang, X., Yu, Q., Wang, S., Wen, X., Bai, S., Cao, L., Zhang, K., Zhang, S., Wang, X., Chen, Z., Cai, Z., & Zhang, G. (2024). Extracellular vesicles derived from M2-like macrophages alleviate acute lung injury in a miR-709-mediated manner. *Journal of Extracellular Vesicles*, *13*, e12437. <https://doi.org/10.1002/jev2.12437>